Role of gut-liver axis in circadian exercise and dietary interventions to improve metabolic health

Kovynev, A.S.

Chapter 5

Exercise training at different intensities induces heat stress, disrupts barrier function and alters microbiota in the gut of mice

Exercise training at different intensities induces heat stress, disrupts barrier function and alters microbiota in the gut of mice

Puqiao Lian[1], Artemiy Kovynev[2,3], Lei Wang[1], Amanda CM Pronk[2,3], Aswin Verhoeven[4], Martin Giera[4], Suzan Thijssen[1], Borja Martínez Téllez[2,3], Sander Kooijman[2,3], Patrick CN Rensen[2,3], Harro Timmerman[5], Harry J Wichers[5], Paul AJ Henricks[1], Gert Folkerts[1], Milena Schönke[2,3,*], Saskia Braber[1,6,*]

[1]Division of Pharmacology, Utrecht Institute for Pharmaceutical Sciences, Faculty of Science, Utrecht University, Utrecht, the Netherlands

[2]Division of Endocrinology, Department of Medicine, Leiden University Medical Center, Leiden, the Netherlands

[3]Einthoven Laboratory for Vascular and Regenerative Medicine, Leiden University Medical Center, Leiden, the Netherlands

[4]Center for Proteomics and Metabolomics, Leiden University Medical Center, Leiden, the Netherlands

[5]Food & Biobased Research, Wageningen University & Research, Wageningen, the Netherlands

[6]Danone Nutricia Research, Utrecht, the Netherlands

*** These authors contributed equally to this work.**

Funding

P.L. was funded by the China Scholarship Council (CSC), grant number 201706210064. M.S. was funded by a grant from the Novo Nordisk Foundation (NNF18OC0032394). A.K. was funded by an LUMC Theme granted to M.S.

Conflicts of interest

The authors declare no conflict of interest. The funder(s) had no role in the design of the study; in the collection, analyses, or interpretation of data; in the writing of the manuscript, or in the decision to publish the results.

Data Availability Statement

The datasets used and/or analysed during the current study are available from the corresponding author on reasonable request.

Keywords: strenuous exercise, heat stress, intestinal epithelial integrity, gut microbiota, short-chain fatty acids

Introduction

Exercise has favourable effects on the human body and its benefits on the musculoskeletal, cardiovascular, and endocrine systems are well-documented [1]. However, an increasing number of studies points to simultaneous adverse effects of exercise on the gastrointestinal (GI) tract and our previous study demonstrated that endurance exercise increases the gut permeability in healthy volunteers [2]. Strenuous exercise, such as marathon running, cycling or triathlon events, is considered a contributing factor to gastrointestinal symptoms and can induce the so-called exercise-induced GI syndrome [3]. This syndrome, characterized by bloating, nausea or diarrhoea, is caused by two distinct pathways: the neuroendocrine-GI pathway and the circulatory-GI pathway [4,5]. The first pathway is associated with an increase in sympathetic activation and a consequent inhibition of GI function. The core of the latter pathway is the redistribution of blood flow to working muscles and peripheral circulation, reducing visceral perfusion. Exercise can lead to a reduction in superior mesenteric artery blood flow by up to 43% in humans [6,7]. This results in local ischemia and hypoxia in the intestine, increasing the production of reactive oxygen species (ROS) and activating signalling pathways that lead to increased gut permeability [8]. Moreover, exercise raises the body core temperature and causes heat stress that activates signalling pathways that reduce epithelial barrier function and causes widespread damage to intestinal epithelium, including shrinking and sloughing of villi [9,10]. Although there is great inter-individual variation, the threshold and degree of intestinal injury may correlate with exercise intensity and environmental temperature [11,12].

The negative impact of strenuous exercise on the GI environment involves disruption of the intestinal epithelial barrier integrity formed by protein complexes

called tight junctions (TJs) and adherens junctions (AJs). These junctional complexes form a “seal” between adjacent cells and act as gatekeeper of the gut barrier. Our previous study showed that combined hypoxic and hyperthermal exposure to co-cultured colonic epithelial cells increases paracellular permeability and activates oxidative stress and heat stress pathways [13]. Heat shock proteins (HSPs), acting as molecular “chaperones” protecting cells from environmental stress, are upregulated under heat stress, assisting with protein synthesis, assembly, and degradation and maintaining the viability and proliferative capacity of cells [14]. Increased HSPs observed in the gut of athletes after endurance competitions prevent TJ breakdown and protect the cytoskeleton of intestinal epithelial cells from hypoxia and hyperthermia-related damage [15,16].

In addition, exercise training modulates the composition of the intestinal microbiota which may affect the normal intestinal function [17,18], however, the underlying mechanisms of this effect remain elusive. This is the first murine study that compares intestinal alterations induced by exercise training at different intensities (moderate and vigorous) and durations (2, 4 and 6 weeks) and investigates the mechanisms behind exercise-induced intestinal injury. The aim was to identify the key regulators of this “destruction and reconstruction process” following exercise.

Materials and Methods

Animals and experimental design

Male C57BL/6J mice at 9 weeks of age were randomly divided into the following groups: control (CON, n = 60), moderate treadmill exercise training (MOD-EX, n = 60), and vigorous treadmill exercise training (VIG-EX, n = 60). In each group, the mice were randomly divided into 3 subgroups by their euthanasia time points: 2, 4, and 6 weeks of intervention (n = 20, respectively). For details see Supplementary Information.

Treadmill running exercise protocol

A 3-day progressive exercise training regime was adapted to familiarize the MOD-EX and VIG-EX mice to a rodent treadmill where the speed and incline of the track were incrementally increased. From day 4 to 15, the mice followed a fixed training regime. To ensure that the exercise straining remained strenuous, starting from

day 15 and day 29, the running speed of the MOD-EX group and the VIG-EX group was increased. The outline of the time points for exercise training, rest and sacrifice are depicted in Supplementary Fig. S1. For details see Supplementary Information.

Euthanasia and intestinal fluorescein permeability

Immediately after the last treadmill training session, FITC-dextran (FD; 4 kDa) was administered to each mouse by oral gavage (500 mg/kg BW). For details see Supplementary Information.

Tissue collection and treatment

Two cm of the segments from the proximal, middle and distal parts of the small intestine and from the colon were isolated and cleaned with ice cold sterile PBS. The spleen was harvested and weighed. Tissue samples were snap-frozen on dry ice and stored at −80°C until future use. Swiss rolls of the intestinal tissue were and then embedded in paraffin blocks for histomorphological evaluation. For details see Supplementary Information.

Western blotting

The colonic segments were lysed and homogenized with cold Pierce RIPA buffer containing a protease inhibitor. For details see Supplementary Information.

Histomorphological evaluation

The Swiss rolls of proximal and distal parts of the small intestine and colonic parts were cut into 5 µm sections and stained with haematoxylin and eosin (H&E). The epithelial morphology, mucosal architecture and inflammation of the intestinal samples were evaluated and scored by double-blinded technicians. For details see Supplementary Information.

Immunofluorescence staining

After standard procedures of gradient rehydration and blocking, the sections were incubated with primary antibody against occludin and then incubated with an Alexa-Fluor fluorescently conjugated secondary antibody. The slides were mounted and counterstained with DAPI. The cells were visualized by a confocal microscopy system. For details see Supplementary Information.

Caecal metabolomics measurement

The concentrations of short-chain fatty acids (SCFAs) and amino acids (AAs) in the caecal contents were quantified by nuclear magnetic resonance spectroscopy. For details see Supplementary Information.

DNA extraction of caecal contents, library construction, gut microbiota sequencing, and bioinformatics analysis

Caecal contents were collected from individual mice and stored at −80°C until future use. For details see Supplementary Information.

Statistical analysis

Statistical analyses were performed by using GraphPad Prism software or the functions of R packages. Differences between groups were determined with parametric repeated measures (RM) two-way analysis of variance (ANOVA), or ordinary one-way ANOVA with Bonferroni post-hoc test, or non-parametric Kruskal-Wallis rank-sum test, two-sided Welch's test, or permutational multivariate analysis of variance (PERMANOVA). A Pearson rank correlation test was conducted to examine associations between the parameters tested, with coefficient $|R| > 0.4$ being considered correlated. Results were considered statistically significant when $p < 0.05$ or corrected $q < 0.05$.

Results

Exercise training increases intestinal leakage and disrupts the intestinal tight junction network in mice

Exercise-induced changes in gut permeability following 2, 4 or 6 weeks of treadmill training were evaluated by measuring the leakage of the fluorescent molecule FITC-Dextran (4 kDa) into the blood after oral administration. Neither moderate (MOD-EX) nor vigorous (VIG-EX) treadmill training affected intestinal FITC-Dextran permeability after 2 weeks of training. Four weeks of MOD-EX, however, significantly increased the serum FITC-Dextran concentration, indicating increased barrier leakage across the intestinal epithelium. After 6 weeks of training, the serum FITC-Dextran concentration was significantly elevated in both MOD-EX and VIG-EX compared to the control mice (CON) (Fig. 1A).

Immunofluorescent staining for TJ protein occludin (OCLN) was conducted to visualize its localization in the colonic villus structures. In the colon of untrained CON mice, OCLN formed a continuous mesh-like pattern in longitudinal villi (Fig. 1B-i) and a clear ring pattern in cross-sectional villi (Fig. 1B-iv). A brush-like appearance of OCLN was observed in compact columnar cells at the tips of the villi in CON (Fig. 1B-i, arrowhead). Exercise training of either intensity induced a disturbed cellular distribution of OCLN and significant loss of columnar cells in mouse colonic villi (Fig. 1B-ii, -iii). Moreover, concentrated protein clusters and a more diffuse and cytosolic distribution were observed in cross sections of the villi (Fig. 1B-v, -vi). In addition, the OCLN localization was evaluated in proximal small intestinal (duodenal) and distal small intestinal (ileal) sections where group differences were less pronounced (Supplementary Fig. S3). OCLN localized at the cell membrane showed continuous chain-like structures forming the rim of normal duodenal and ileal villi in CON, which is less clear following exercise training (Supplementary Fig S3).

The changes in the TJ network after exercise were confirmed by Western blotting. Both MOD-EX and VIG-EX decreased OCLN protein expression in the mouse colon (Fig. 1C). In addition, the protein expression of ZO-1 significantly decreased in MOD-EX, while VIG-EX did not affect ZO-1 expression but enhanced CLDN3 expression (Fig. 1D, E).

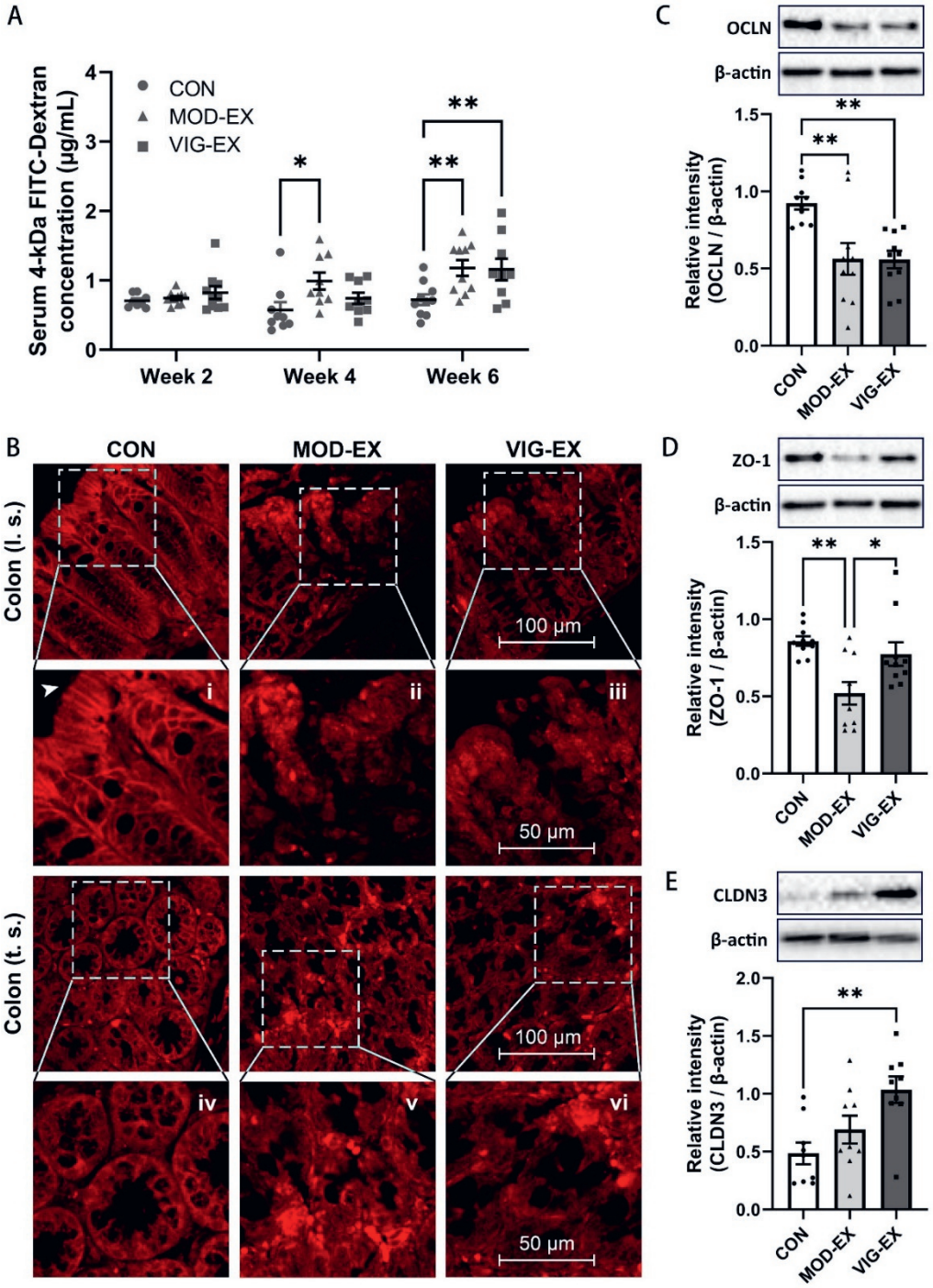
A
Serum 4-kDa FITC-Dextran concentration (μg/mL)
CON
MOD-EX
VIG-EX
Week 2
Week 4
Week 6
B
CON
MOD-EX
VIG-EX
Colon (l. s.)
Colon (t. s.)
100 μm
50 μm
i
ii
iii
iv
v
vi
C
OCLN
β-actin
Relative intensity (OCLN / β-actin)
D
ZO-1
β-actin
Relative intensity (ZO-1 / β-actin)
E
CLDN3
β-actin
Relative intensity (CLDN3 / β-actin)

Figure 1. Effect of exercise on intestinal barrier function. (**A**) Serum 4-kDa FITC-Dextran concentration 1 h after oral gavage following 2, 4 and 6 weeks of exercise training. Data are presented as mean ± SEM; n = 9 (VIG-EX of Week 6) or n = 10 (other groups) per group. Statistical differences were analysed by one-way ANOVA followed by Bonferroni's multiple comparison test. (**B**) Immunofluorescence staining of colonic occludin protein after 6 weeks of exercise training. The results were acquired by Leica TCS SP8 confocal microscope with HCX IRAPO L 25×/0.95 objective lens at 2.25× digital magnification; pinhole: 1.50 AU. Red colour: fluorescent signals from Alexa-Fluor 594 secondary antibodies. (**C**, **D**, **E**) Relative protein expression of colonic claudin-3, occludin and ZO-1 after 6 weeks of exercise training, assessed by Western blot. All target proteins were normalized to reference protein β-actin. Data are presented as mean ± SEM; n = 9-10 per group. Statistical differences were analysed by one-way ANOVA followed by Bonferroni's multiple comparison test. * $p < 0.05$, ** $p < 0.01$. CON: Control; MOD-EX: moderate exercise; VIG-EX: vigorous exercise; l.s.: longitudinal section; t.s.: transverse section; OCLN: occludin; ZO-1: zonula occludens-1; CLDN3: claudin-3.

Exercise elevates rectal temperature and induces a heat stress response in mouse colon

The thermal effects of exercise on the mouse intestine were determined by measuring rectal temperature and the expression of heat shock-related proteins/transcription factors. During the 6 weeks of treadmill training, the rectal temperature of CON narrowly fluctuated around the baseline (37.8 ± 0.1°C, mean ± SEM, sic passim) within approx. 0.5°C (Fig. 2A). The rectal temperatures of MOD-EX and VIG-EX were significantly increased 15 min after exercise compared to CON and reached 39.0 ± 0.1°C and 38.7 ± 0.1°C, respectively, at week 6 (Fig. 2A). However, the rectal temperature between the two exercise groups was not significantly different.

At week 6, after the final running session, the mouse colon tissue was collected and the protein levels of HSP-70, the conserved ubiquitously expressed protein of the heat shock protein family, and the transcription factor HSF-1, the primary mediator of transcriptional responses to heat stress, were determined. Both MOD-EX and VIG-EX significantly enhanced the abundance of HSF-1 in the colon (Fig. 2B). Correspondingly, the protein abundance of chaperone HSP-70 was increased

in both exercise groups, without significant differences between MOD-EX and VIG-EX (Fig. 2C).

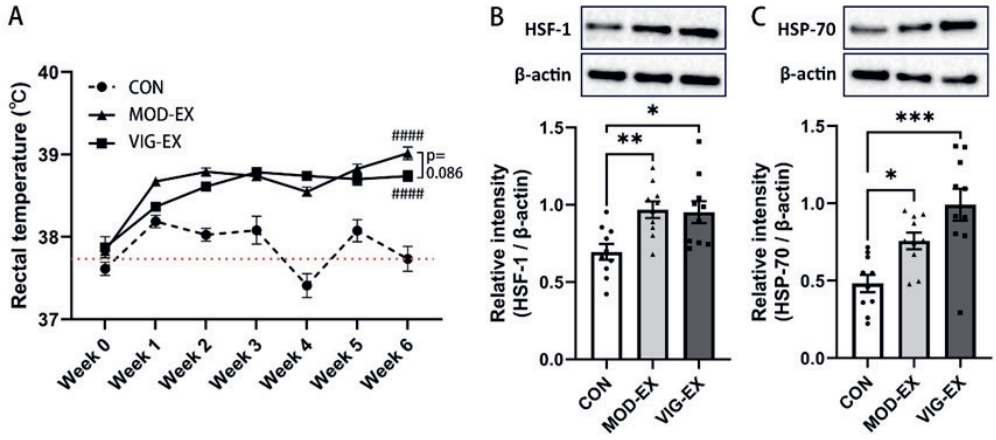

Figure 2. The effect of exercise on the intestinal heat stress response. (**A**) Weekly post-exercise (after 15 min) rectal temperatures of mice acquired by a rectal thermometer. The dotted red line represents the average rectal temperature of all groups. Data are presented as mean ± SEM; n = 20 per group. Statistical differences were analysed by repeated measures two-way ANOVA. #### $p < 0.0001$ vs Control. Relative protein expression of (**B**) HSF-1 and (**C**) HSP70 in the colon after 6 weeks of exercise training assessed by Western blot. The target proteins were normalized to reference protein β-actin. Data are presented as mean ± SEM; n = 10 per group. Statistical differences were analysed by one-way ANOVA followed by Bonferroni's multiple comparison test. * $p < 0.05$, ** $p < 0.01$, *** $p < 0.001$. CON: Control; MOD-EX: moderate exercise; VIG-EX: vigorous exercise; HSP: heat shock protein; HSF: heat shock factor.

Exercise training alters intestinal morphology and induces local intestinal inflammation in mice

Following 6 weeks of training, proximal and distal small intestine and colonic sections were examined to determine the effect of exercise training on intestinal histomorphology. In CON, limited inflammatory infiltration was observed. CON showed well-distended villi from base to tip in the proximal small intestine (duodenum), distal small intestine (ileum) and colon, and the mucosal and

submucosal architecture was intact (Fig. 3A, B). Intestinal villus length is correlated to the digestive and absorptive functions of the intestine, as it affects surface area of the digestive tract [19]. The duodenal villus length was significantly shorter in MOD-EX compared to CON (Fig. 3C, D), while this effect was less pronounced in VIG-EX. No significant changes in villus length were observed in the ileum after exercise training (Fig. 3D), but blunted and deformed villi were distinct characteristics in the duodenum and ileum (Fig. 3A, asterisk) of both exercise groups.

However, significantly fewer goblet cells were counted in the ileum of VIG-EX, suggesting a possibly impaired mucus production, while no significant differences were observed between MOD-EX and CON (Fig. 3E). No significant changes in the number of goblet cells were observed in the duodenum after exercise training (Fig. 3E).

In MOD-EX and VIG-EX, mucosal or submucosal infiltration of leukocytes combined with occasional intestinal haemorrhage was detected in the duodenum, ileum and colon (Fig. 3A, solid arrows, and arrowheads). Additionally, in MOD-EX, ulceration and submucosal widening were observed in all parts of the intestine of MOD-EX (Fig. 3A, Uc) and submucosal widening and submucosal oedema were observed in duodenal, ileal and colonic sections in VIG-EX (Fig. 3A, asterisks, solid arrows, dashed arrows and Sw). These alterations caused a significantly higher morphological score of duodenum and ileum in MOD-EX and VIG-EX and of colon in MOD-EX compared to CON (Fig. 3B).

Interestingly, the serum concentration of CRP, a marker for global inflammation secreted by the liver, was increased following 6 weeks of MOD-EX (Supplementary Fig. S4A) but not VIG-EX, suggesting mildly elevated systemic inflammation with MOD-EX. However, quantification of several circulating cytokines/chemokines showed that the levels of pro-inflammatory G-CSF, CXCL1 and CCL2 were not significantly different between the groups (Supplementary Fig. S4B-D). Spleen/body weight ratios were also not different between the groups (Supplementary Fig. S5C).

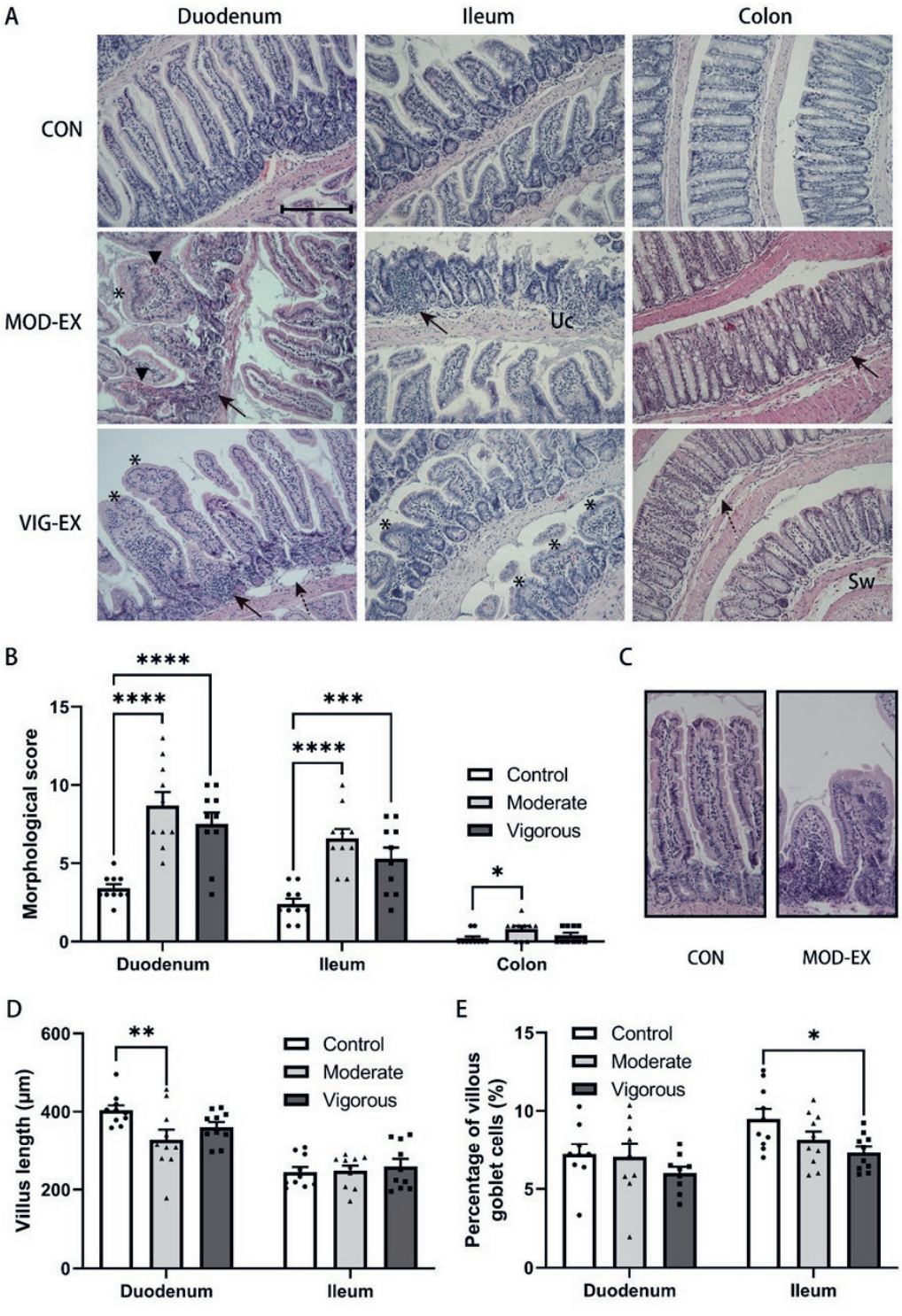
A
Duodenum
Ileum
Colon
CON
MOD-EX
VIG-EX
Uc
Sw
B
Morphological score
Control
Moderate
Vigorous
Duodenum
Ileum
Colon
C
CON
MOD-EX
D
Villus length (μm)
Control
Moderate
Vigorous
Duodenum
Ileum
E
Percentage of villous goblet cells (%)
Control
Moderate
Vigorous
Duodenum
Ileum

Figure 3. Effect of exercise training on intestinal morphology and inflammation. (**A**) Representative images of H&E-stained proximal small intestinal (duodenal), distal small intestinal (ileal), and colonic sections of mice after 6 weeks of exercise training illustrate the inflammatory cell infiltration, epithelial changes and altered mucosa architecture. The images were acquired by Olympus BX50 microscope with UPlanFI 20× /0.25 objective lens and Leica DFC320 10× camera (200×, scale bar 200 µm). Solid arrow: mucosal or submucosal infiltration of leukocytes; dashed arrow: submucosal oedema; arrowhead: haemorrhage; Uc: ulceration; asterisk: blunted villus; Sw: submucosal widening. (**B**) Histological scores of intestinal morphology based on inflammatory cell infiltration, epithelial changes and altered mucosa architecture. (**C**) Representative images of cross-sectioned duodenal villi (**D**) Villus lengths measured by ImageJ software. (**E**) Percentages of villus goblet cells counted after Alcian Blue/Nuclear Fast Red staining. Data are presented as mean ± SEM; n = 10 mice per group. Statistical differences were analysed by one-way ANOVA followed by the Bonferroni's multiple comparison test. ** $p < 0.01$, *** $p < 0.001$, **** $p < 0.0001$. CON: Control; MOD-EX: moderate exercise; VIG-EX: vigorous exercise.

Vigorous but not moderate exercise training affects caecal metabolite levels

Following 6 weeks of exercise training, caecal contents were collected and the concentrations of the six most abundant SCFAs (formate, acetate, propionate, butyrate, isobutyrate and valerate), lactate and four amino acids that are universally utilized by gut microbes to produce SCFAs (alanine, methionine, valine and threonine) were determined 1 h after the final exercise bout. VIG-EX, but not MOD-EX, increased caecal levels of acetate, butyrate and propionate (Fig. 4B-D), but decreased formate and valerate concentrations (Fig. 4A, F). VIG-EX for 6 weeks decreased the levels of amino acids in the cecum, including alanine, methionine, valine and threonine (Fig. 4H-K). Accordingly, total concentration of SCFAs and AAs in VIG-EX was significantly changed compared to CON and MOD-EX (Fig. 4L, M). Neither training program affected the caecal levels of lactate (Fig. 4G). Notably, there was no significant difference in the average daily food intake and cumulative food intake over 6 weeks between the groups (Supplementary Fig. S6).

Both MOD-EX and VIG-EX significantly increased the protein expression of G-protein-coupled receptor (GPR) 41 and GPR43, the main mammalian receptors of

SCFAs, in colon compared to CON (Fig. 4N, O). Moreover, VIG-EX increased the expression of GPR41 to a greater extent than MOD-EX.

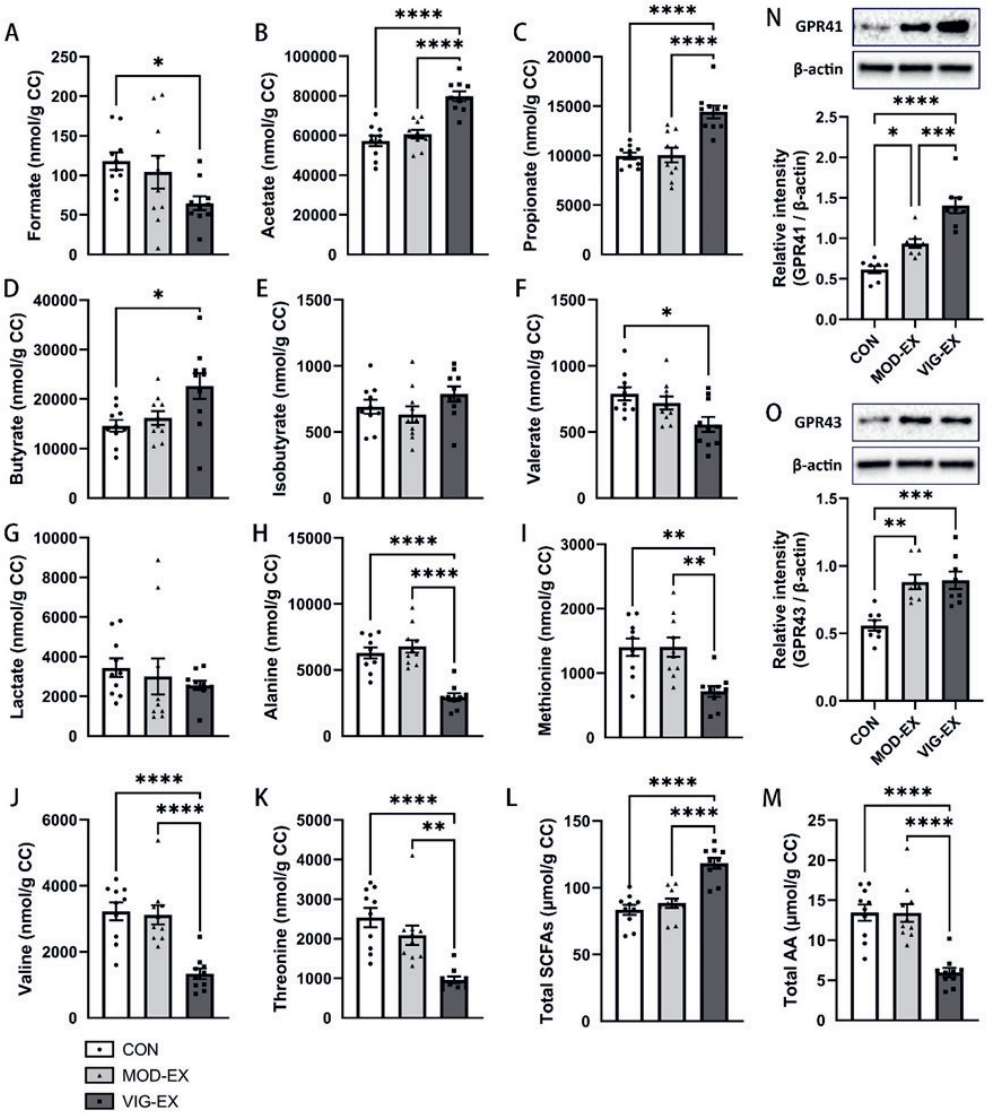

Figure 4. The effect of exercise on caecal metabolite levels. Concentrations of short-chain fatty acids (**A** - **F**), lactate (**G**), and amino acids (**H** - **K**) in caecal contents after 6 weeks of exercise training measured 1 h after the last training bout by nuclear magnetic resonance spectroscopy. (**L**, **M**) Concentrations of total short-chain fatty acids and total amino acids in caecal contents after 6 weeks of exercise training measured 1 h after the last training bout. (**N**, **O**) The effect of

strenuous exercise on colonic G-protein-coupled receptors 41 and 43. Relative protein expression of GPR41 and GPR43 in the murine colon after 6 weeks of exercise assessed by Western blot. All target proteins were normalized to reference protein β-actin. Data in the bar plots are presented as mean ± SEM; n = 10 per group. Statistical differences were analysed by one-way ANOVA followed by the Bonferroni's multiple comparison test. * $p < 0.05$, ** $p < 0.01$, *** $p < 0.001$, **** $p < 0.0001$. CC: caecal contents; CON: Control; MOD-EX: moderate exercise; VIG-EX: vigorous exercise; SCFAs: short-chain fatty acids; AAs: amino acids; GPR: G-protein-coupled receptor.

Exercise training promotes changes in microbiota diversity

After 6 weeks of exercise training, the effect on the composition of the murine gut microbiota was evaluated. Significant differences in alpha diversity, showing the diversity within an individual sample, and beta diversity, showing the (dis-)similarities of the microbiomes of different groups, were evident in MOD-EX and VIG-EX when compared to CON ($p = 0.001$). However, the two exercise groups did not significantly differ from each other in alpha or beta diversity (Fig. 5A, B).

The microbiome of all groups was dominated by bacteria belonging to the phylae Bacteroidota or Firmicutes, and MOD-EX and VIG-EX only caused a decrease of Actinobacteriota (from 2.31 ± 0.90% to 0.02 ± 0.00% and 0.03 ± 0.01%, respectively) (Fig. 5C). However, the microbial composition of MOD-EX and VIG-EX differed from that of CON at family level. Lactobacillaceae accounted for 10.3 ± 4.0% of total caecal bacteria in CON but their abundance was reduced to less than 1% in MOD-EX and VIG-EX (Fig. 5D).

Microbiome taxonomic abundance was further analysed using LEfSe analyses which identifies discriminating bacterial taxa between groups based on statistical significance and biological relevance. Results were ranked by their linear discriminant analysis (LDA) score. Also here, the abundance of Lactobacillaceae (of the phylum Firmicutes) was identified as the main distinction in CON, whereas in MOD-EX and VIG-EX the strongest associations were related to Rikenellaceae (of the phylum Bacteroidota) and Lachnospiraceae (of the phylum Firmicutes), respectively (Supplementary Fig. S8). When analysing the taxa below family level, Prevotellaceae UCG-001 from the phylum Bacteroidota was identified as the most

enriched genus in MOD-EX, followed by Rikenellaceae RC9 (Supplementary Fig. S9, S10). In VIG-EX, Lachnospiraceae UCG-001 and the family members Roseburia, ASF356 and Acetatifactor were identified as the most enriched genera (Supplementary Fig. S9, S10). Pearson's correlation analyses were carried out between the relative microbiota abundance and the intestinal permeability measured with FITC-Dextran. Three species from the family of Lachnospiraceae and the genus Butyricicoccus were found to positively correlate with the serum FITC-dextran concentration ($p \leq 0.01$, Fig. 5E-G), indicating a link between these species and intestinal permeability.

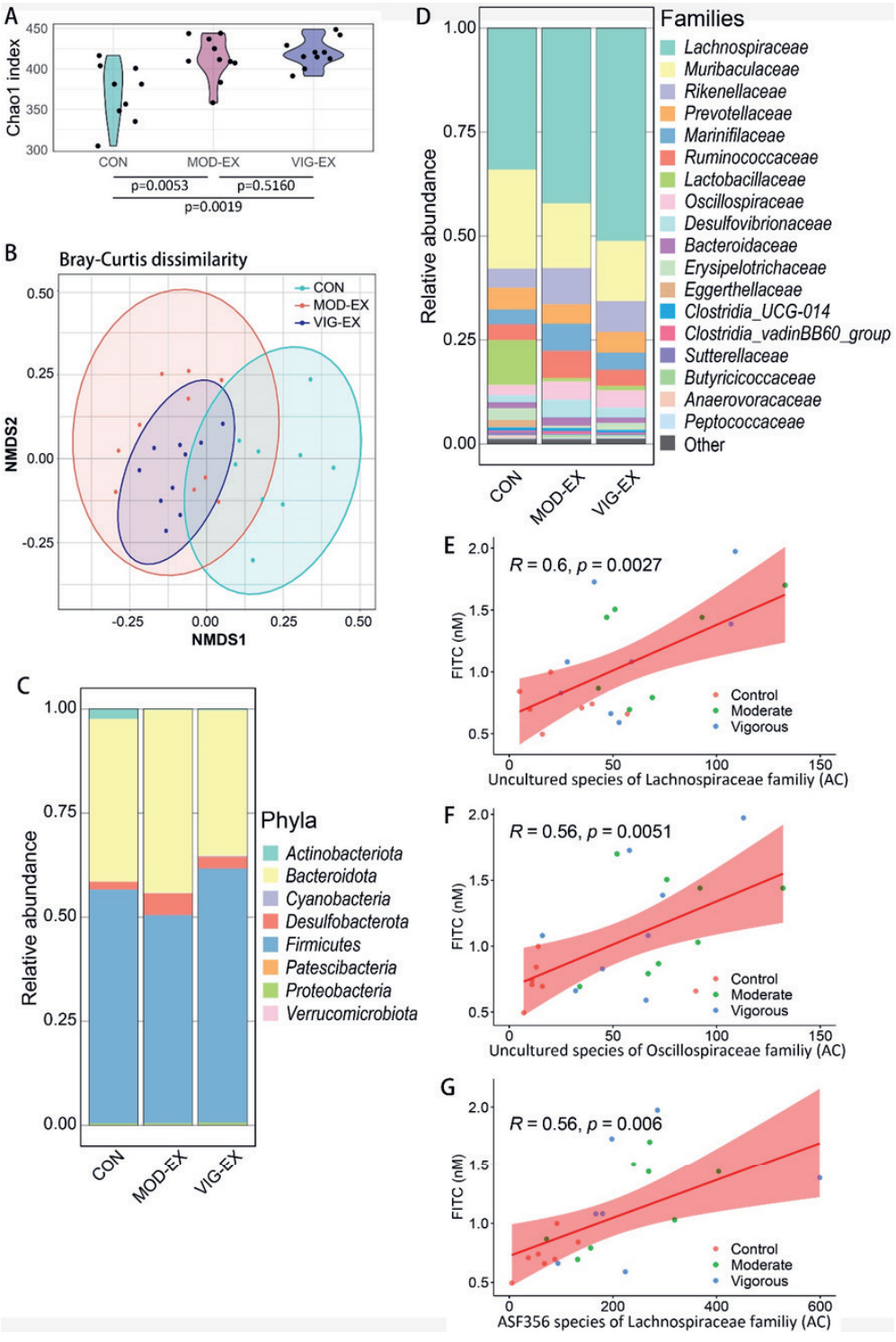
A
Chao1 index
450
400
350
300
CON
MOD-EX
VIG-EX
p=0.0053
p=0.5160
p=0.0019
B
Bray-Curtis dissimilarity
CON
MOD-EX
VIG-EX
NMDS2
NMDS1
0.50
0.25
0.00
-0.25
C
Relative abundance
1.00
0.75
0.50
0.25
0.00
Phyla
Actinobacteriota
Bacteroidota
Cyanobacteria
Desulfobacterota
Firmicutes
Patescibacteria
Proteobacteria
Verrucomicrobiota
D
Families
Lachnospiraceae
Muribaculaceae
Rikenellaceae
Prevotellaceae
Marinifilaceae
Ruminococcaceae
Lactobacillaceae
Oscillospiraceae
Desulfovibrionaceae
Bacteroidaceae
Erysipelotrichaceae
Eggerthellaceae
Clostridia_UCG-014
Clostridia_vadinBB60_group
Sutterellaceae
Butyricicoccaceae
Anaerovoracaceae
Peptococcaceae
Other
E
R = 0.6, p = 0.0027
FITC (nM)
Control
Moderate
Vigorous
Uncultured species of Lachnospiraceae familiy (AC)
F
R = 0.56, p = 0.0051
FITC (nM)
Uncultured species of Oscillospiraceae familiy (AC)
G
R = 0.56, p = 0.006
FITC (nM)
ASF356 species of Lachnospiraceae familiy (AC)

Figure 5. The effect of exercise training on caecal microbiota diversity and composition. (**A**) Alpha diversity depicted as Chao1 index. (**B**) Beta diversity depicted as NMDS plot based on Bray–Curtis dissimilarity matrix. Each point represents a single sample and the closed areas represent confidence ellipses. The statistical significance among the groups is determined with permutational multivariate analysis of variance (PERMANOVA), adjusted for exercise status. (**C**, **D**) Bacterial taxonomic composition in the mouse cecum following 6 weeks of exercise training at phylum and family levels. The relative abundances are displayed as mean of samples. "Other" in (D) includes all the families with less than 0.2% abundance and unidentified families. (**E**, **F**, **G**) Pearson's correlation analyses between the specific gut microorganism abundance and serum FITC-dextran concentration of CON, MOD-EX and VIG-EX. n = 9 (CON) or 10 (MOD-EX and VIG-EX). CON: Control; MOD-EX: moderate exercise; VIG-EX: vigorous exercise; NMDS: non-metric multi-dimensional scaling; AC : abundance counts.

Discussion

Strenuous exercise can dysregulate the intestinal homeostasis that is tightly linked to the function of the intestinal barrier, affecting nutrient absorption and the defence against pathogens and toxins [20]. Here we investigated the intestinal alterations induced by exercise training of different intensities (moderate and vigorous) and outlined the mechanisms behind exercise-induced intestinal injury. This study found that continuous moderate intensity exercise imposed greater damage on the mouse intestine than vigorous intensity exercise with intermittent rest days. Increased intestinal SCFA production observed with vigorous exercise training may hereby have compensated the exercise-induced intestinal damage.

In this study, the difference in exercise intensity was reflected in different average running speeds, durations and frequencies. The average running speed of VIG-EX was 43-49% higher than that of MOD-EX but VIG-EX only ran 30% of the MOD-EX running time. This resulted in a lower total distance run by VIG-EX compared to MOD-EX (11,835 m vs 26,174 m). Notably, 4 weeks of MOD-EX (16,674 m) was sufficient to increase intestinal permeability, which was first observed at week 6 in VIG-EX (11,835 m). Substantial differences in running speed and distance may lead to distinct changes in energy metabolism, which can be the underlying cause of the differences observed in intestinal parameters (e.g. microbiota composition and metabolite levels) between the two exercise groups. Exercise training can

modulate energy metabolism by affecting caloric intake and our recent study indeed demonstrated that mice that trained at a moderate treadmill running speed ate more high fat high cholesterol diet than untrained mice [17]. Strenuous exercise in humans, on the other hand, suppresses appetite and food intake [21]. Here, no significant differences in body weight or food intake between the groups were observed. As we did not assess the feeding events throughout training and rest days separately, we cannot exclude that different exercise training intensities affected dietary patterns.

As a response to heat stress during exercise, heart rate and blood flow are increased to accelerate heat dissipation. Molecular chaperones, such as heat shock proteins HSP-70 and HSP-90, dissociate from HSF-1 to perform their reparative roles by assisting protein refolding and by promoting the degradation of misfolded proteins [22]. This also allows HSF-1 to stimulate the transcription of target genes that help to cope with such proteotoxic stress [23]. We observed that the expression of HSP-70 and HSF-1 in the colon was elevated one hour after the final training, indicating that the effect of heat stress caused by both moderate and vigorous exercise continues after exercising and may cause (intestinal) tissue damage. Interestingly, after 6 weeks, only MOD-EX elevated the level of serum CRP, potentially suggesting more severe intestinal damage and systemic inflammation following moderate rather than vigorous exercise training. This was in line with elevated morphological scores and significantly shortened villi with MOD-EX. However, circulating pro-inflammatory cytokines and chemokines were undetectable or not significantly elevated after 6 weeks, indicating overall low systemic inflammation in these healthy mice. It may be of interest to study the inflammatory response to moderate and vigorous exercise over time to establish whether CRP levels in MOD-EX subside after an initial induction or whether VIG-EX also elevates circulating CRP after a longer training period. Here, it would also be meaningful to assess whether the frequency of intermittent rest days can modulate whole-body and intestinal inflammation and whether these effects are directly linked to the intestinal barrier function. A clinical study showed a link between exercise intensity and small intestinal permeability, however, all groups trained at the same frequency, making it difficult to assess the importance of rest days in the recovery of the intestine [12]. Of note, high-intensity interval training was found to have superior beneficial effects on cardiovascular function and the metabolic syndrome compared to moderate intensity continuous training [71,72].

Nonetheless, clinical studies on the effects of exercise intensity and frequency on intestinal injury and pro-inflammatory disease drivers are lacking.

Functionally, both MOD-EX and VIG-EX after 6 weeks increased intestinal leakage which correlated positively with rectal temperature. This increase in intestinal permeability is likely causally linked to impaired intestinal epithelial tight junction expression and localization. After 6 weeks of exercise training that induced elevated rectal temperatures, occludin and ZO-1 protein expression was lower in MOD-EX colon compared to CON, implicating heat stress as the causal factor. Another in vivo study also showed that heat stress can induce severe intestinal barrier damage [24]. Interestingly, claudin-3 protein expression increased after 6 weeks of exercise. This might be a compensatory mechanism to help maintain the integrity of the tight junctions, since Poritz et al. demonstrated that the increase of claudin-1 compensated the loss of ZO-1 in a murine colitis model [25]. In vitro we previously observed an increase of AJ protein E-cadherin, accompanied by a decrease of the TJ proteins ZO-1, claudin-3 and occludin, in a hypoxia- and heat-exposed Caco-2/HT-29 co-culture model [13]. Conversely, several other studies described an exercise-induced upregulation of TJ proteins (e.g. claudin-1, claudin-5 and occludin) as markers of enhanced barrier function in the gut and even in other organs with mild exercise [26]. Together, these studies highlight the complexity of the intestinal tight junction network in response to physical exercise.

Both intensities of exercise training altered the the gut microbiota composition which may directly affect the integrity of the intestinal epithelium. For example, the effects of Lactobacillus and its derivatives on preserving TJ protein expression and distribution in the intestinal tract have been proven in various in vivo and ex vivo studies [27–29]. Here, both intensities of exercise training diminished the presence of caecal Lactobacillus, potentially contributing to the observed intestinal barrier disruption. In future studies, Lactobacillus-enriched diets or gut microbiota transplants could be introduced to observe whether the addition of Lactobacillus can counteract the intestinal leakage from moderate to vigorous exercise training.

SCFAs are the products of microbial fermentation of non-digestible oligosaccharides [30,31]. These metabolites, like butyrate, can improve gut barrier function by enhancing mucin and TJ protein ZO-1, occludin and claudin-1 expression [32,33], and exert a general protective effect on the host by enhancing

immunity and their anti-inflammatory capacity under stress [34–37]. Bacteria such as Lachnospiraceae, Prevotellaceae, and Butyricicoccaceae, which are strongly associated with SCFA production [38], were significantly more abundant in both exercise groups. This may arise from the decrease of commensal lactobacilli, lifting the inhibitory effect of environmental acidification on the growth of e.g. Lachnospiraceae [39]. Moreover, the increased activity of endogenous antioxidants after SCFA supplementation has been demonstrated in in vitro and in vivo studies [40,41], suggesting that SCFAs also modulate the oxidative stress pathways. The increase of SCFA production in the gut may also contribute to increased muscle strength/growth and whole-body energy expenditure through increased fatty acid oxidation [42–44], or interact specifically with GPR41 and GPR43, stimulating the secretion of incretins involved in whole-body metabolism [45,46]. This underlines the important reciprocal link between SCFAs and whole-body homeostasis. In fact, VIG-EX, with increased abundance of Lachnospiraceae spp. and significantly elevated SCFAs, which correlated with GPR41 and 43 expression levels [47], demonstrated less severe intestinal damage than MOD-EX. Accordingly, we speculate that exercise training with intermittent rest days (VIG-EX) is more favourable (or less harmful) to the colonization and reproduction of these SCFA-producing species than daily exercise (MOD-EX). While exercise can cause intestinal epithelial damage and activation of HSPs, changes to the microbiota composition and the enhanced production of SCFAs may be part of the positive adaptation to chronic exercise training that compensate for exercise-induced GI stress.

In addition, 6 weeks of VIG-EX significantly reduced caecal amino acid concentrations. This decrease could be related to increased intestinal leakiness or associated with elevated SCFA production, since total caecal SCFAs correlated negatively with total caecal amino acids. Amino acids can be utilized by intestinal microorganisms to synthesize structural proteins and serve as precursors of SCFAs [48]. Increased leakiness, on the other hand, could also promote increased influx of muscle-derived lactate during exercise that can also serve as precursor of microbially produced SCFAs, thus providing extra energy by subsequent fatty acid oxidation [49]. As no significantly increased caecal lactate levels were observed after exercise, it can be speculated that lactate was quickly converted and/or metabolized soon after exercise. Lactate production increases significantly with increasing running speed in mice [50]. In line, we speculate that in VIG-EX, higher

circulating lactate levels during and immediately after the vigorous exercise contributed to the increased SCFA production. This and other exercise-induced fluxes of metabolites and their effect on gut microbes should be investigated further.

In summary (Fig. 6), exercise elevated the core body temperature, leading to heat stress and increased intestinal epithelial permeability characterized by disruption of the TJ network. Meanwhile, exercise training also altered the gut microbiota and reduced the abundance of Lactobacillaceae that may have contributed to the deteriorated intestinal status, indicating a novel cause of intestinal injury from exercise training. On the other hand, exercise training increased the abundance of SCFA-producing bacteria such as Lachnospiraceae, potentially as a compensatory response to alleviate intestinal injury.

Acknowledgements

We wish to gratefully acknowledge the technical and intellectual support provided by our colleagues (in alphabetical order by last names) Ingrid van Ark, Tiago Cardoso, Mara Diks, Gemma Dingjan, Thea Leusink-Muis, Lucía Peralta, Elena Sendino, Negisa Seyedtoutounchi, Koen Westphal, Yi Yang, Yuanpeng Zheng and Marit Zuurveld at Utrecht Institute of Pharmaceutical Sciences (UIPS), Utrecht University, The Netherlands.

References

1. Ruegsegger, G.N.; Booth, F.W. Health Benefits of Exercise. Cold Spring Harb Perspect Med 2018, 8, doi:10.1101/CSHPERSPECT.A029694.
2. JanssenDuijghuijsen, L.M.; Mensink, M.; Lenaerts, K.; Fiedorowicz, E.; van Dartel, D.A.M.; Mes, J.J.; Luiking, Y.C.; Keijer, J.; Wichers, H.J.; Witkamp, R.F.; et al. The Effect of Endurance Exercise on Intestinal Integrity in Well-Trained Healthy Men. Physiol Rep 2016, 4, doi:10.14814/PHY2.12994.
3. de Oliveira, E.P.; Burini, R.C.; Jeukendrup, A. Gastrointestinal Complaints During Exercise: Prevalence, Etiology, and Nutritional Recommendations. Sports Med 2014, 44, 79, doi:10.1007/S40279-014-0153-2.
4. Ribeiro, F.M.; Petriz, B.; Marques, G.; Kamilla, L.H.; Franco, O.L. Is There an Exercise-Intensity Threshold Capable of Avoiding the Leaky Gut? Front Nutr 2021, 8, 627289, doi:10.3389/FNUT.2021.627289.
5. Costa, R.J.S.; Snipe, R.M.J.; Kitic, C.M.; Gibson, P.R. Systematic Review: Exercise-Induced Gastrointestinal Syndrome—Implications for Health and Intestinal Disease. Aliment Pharmacol Ther 2017, 46, 246–265, doi:10.1111/APT.14157.
6. Qamar, M.I.; Read, A.E. Effects of Exercise on Mesenteric Blood Flow in Man. Gut 1987, 28, 583–587, doi:10.1136/GUT.28.5.583.
7. Perko, M.J.; Nielsen, H.B.; Skak, C.; Clemmesen, J.O.; Schroeder, T. v.; Secher, N.H. Mesenteric, Coeliac and Splanchnic Blood Flow in Humans during Exercise. J Physiol 1998, 513, 907, doi:10.1111/J.1469-7793.1998.907BA.X.
8. Keirns, B.H.; Koemel, N.A.; Sciarrillo, C.M.; Anderson, K.L.; Emerson, S.R. Exercise and Intestinal Permeability: Another Form of Exercise-Induced Hormesis? Am J Physiol Gastrointest Liver Physiol 2020, 319, G512–G518, doi:10.1152/AJPGI.00232.2020/ASSET/IMAGES/LARGE/ZH30102078410001.JPEG.
9. Ortega, A.D.S.V.; Szabó, C. Adverse Effects of Heat Stress on the Intestinal Integrity and Function of Pigs and the Mitigation Capacity of Dietary Antioxidants: A Review. Animals 2021, Vol. 11, Page 1135 2021, 11, 1135, doi:10.3390/ANI11041135.
10. Santos, R.R.; Awati, A.; Roubos-van den Hil, P.J.; Tersteeg-Zijderveld, M.H.G.; Koolmees, P.A.; Fink-Gremmels, J. Quantitative Histo-Morphometric Analysis of Heat-Stress-Related Damage in the Small Intestines of Broiler Chickens. Avian Pathology 2015, 44, 19–22,

doi:10.1080/03079457.2014.988122/SUPPL_FILE/CAVP_A_988122_SM6225.DOCX
.
11. Yeh, Y.J.; Law, L.Y.L.; Lim, C.L. Gastrointestinal Response and Endotoxemia during Intense Exercise in Hot and Cool Environments. Eur J Appl Physiol 2013, 113, 1575–1583, doi:10.1007/S00421-013-2587-X/FIGURES/4.
12. Pals, K.L.; Chang, R.T.; Ryan, A.J.; Gisolfi, C. v. Effect of Running Intensity on Intestinal Permeability. J Appl Physiol 1997, 82, 571–576, doi:10.1152/JAPPL.1997.82.2.571/ASSET/IMAGES/LARGE/JAPP0523305.JPEG.
13. Lian, P.; Braber, S.; Varasteh, S.; Wichers, H.J.; Folkerts, G. Hypoxia and Heat Stress Affect Epithelial Integrity in a Caco-2/HT-29 Co-Culture. Sci Rep 2021, 11, doi:10.1038/S41598-021-92574-5.
14. Radons, J. The Human HSP70 Family of Chaperones: Where Do We Stand? Cell Stress Chaperones 2016, 21, 379, doi:10.1007/S12192-016-0676-6.
15. Fehrenbach, E.; Niess, A.M.; Schlotz, E.; Passek, F.; Dickhuth, H.H.; Northoff, H. Transcriptional and Translational Regulation of Heat Shock Proteins in Leukocytes of Endurance Runners. J Appl Physiol (1985) 2000, 89, 704–710, doi:10.1152/JAPPL.2000.89.2.704.
16. Fehrenbach, E.; Passek, F.; Niess, A.M.; Pohla, H.; Weinstock, C.; Dickhuth, H.H.; Northoff, H. HSP Expression in Human Leukocytes Is Modulated by Endurance Exercise. Med Sci Sports Exerc 2000, 32, 592–600, doi:10.1097/00005768-200003000-00007.
17. Schönke, M.; Ying, Z.; Kovynev, A.; In het Panhuis, W.; Binnendijk, A.; van der Poel, S.; Pronk, A.C.M.; Streefland, T.C.M.; Hoekstra, M.; Kooijman, S.; et al. Time to Run: Late Rather than Early Exercise Training in Mice Remodels the Gut Microbiome and Reduces Atherosclerosis Development. FASEB J 2023, 37, doi:10.1096/FJ.202201304R.
18. Monda, V.; Villano, I.; Messina, A.; Valenzano, A.; Esposito, T.; Moscatelli, F.; Viggiano, A.; Cibelli, G.; Chieffi, S.; Monda, M.; et al. Exercise Modifies the Gut Microbiota with Positive Health Effects. Oxid Med Cell Longev 2017, 2017, doi:10.1155/2017/3831972.
19. Helander, H.F.; Fändriks, L. Surface Area of the Digestive Tract – Revisited. http://dx.doi.org/10.3109/00365521.2014.898326 2014, 49, 681–689, doi:10.3109/00365521.2014.898326.
20. Lian, P.; Braber, S.; Garssen, J.; Wichers, H.J.; Folkerts, G.; Fink-Gremmels, J.; Varasteh, S. Beyond Heat Stress: Intestinal Integrity Disruption and Mechanism-Based Intervention Strategies. Nutrients 2020, 12, 734.

21. Dorling, J.; Broom, D.R.; Burns, S.F.; Clayton, D.J.; Deighton, K.; James, L.J.; King, J.A.; Miyashita, M.; Thackray, A.E.; Batterham, R.L.; et al. Acute and Chronic Effects of Exercise on Appetite, Energy Intake, and Appetite-Related Hormones: The Modulating Effect of Adiposity, Sex, and Habitual Physical Activity. Nutrients 2018, 10, doi:10.3390/NU10091140.
22. Whitley, D.; Goldberg, S.P.; Jordan, W.D. Heat Shock Proteins: A Review of the Molecular Chaperones. J Vasc Surg 1999, 29, 748–751, doi:10.1016/S0741-5214(99)70329-0.
23. Zhang, Y.; Chou, S.D.; Murshid, A.; Prince, T.L.; Schreiner, S.; Stevenson, M.A.; Calderwood, S.K. The Role Of Heat Shock Factors In Stress-Induced Transcription. Methods Mol Biol 2011, 787, 21, doi:10.1007/978-1-61779-295-3_2.
24. Koch, F.; Thom, U.; Albrecht, E.; Weikard, R.; Nolte, W.; Kuhla, B.; Kuehn, C. Heat Stress Directly Impairs Gut Integrity and Recruits Distinct Immune Cell Populations into the Bovine Intestine. Proc Natl Acad Sci U S A 2019, 116, 10333–10338, doi:10.1073/PNAS.1820130116/SUPPL_FILE/PNAS.1820130116.SD05.XLSX.
25. Poritz, L.S.; Garver, K.I.; Green, C.; Fitzpatrick, L.; Ruggiero, F.; Koltun, W.A. Loss of the Tight Junction Protein ZO-1 in Dextran Sulfate Sodium Induced Colitis. Journal of Surgical Research 2007, 140, 12–19, doi:10.1016/J.JSS.2006.07.050.
26. Shin, H.E.; Kwak, S.E.; Zhang, D. di; Lee, J.; Yoon, K.J.; Cho, H.S.; Moon, H.Y.; Song, W. Effects of Treadmill Exercise on the Regulation of Tight Junction Proteins in Aged Mice. Exp Gerontol 2020, 141, 111077, doi:10.1016/J.EXGER.2020.111077.
27. Liu, J.; Li, R.; Liu, P.; Ruiz, J.; Qin, D.; Ma, Y.; Wang, Y.; Hou, X.; Yu, L. Contribution of Lactobacilli on Intestinal Mucosal Barrier and Diseases: Perspectives and Challenges of Lactobacillus Casei. Life 2022, Vol. 12, Page 1910 2022, 12, 1910, doi:10.3390/LIFE12111910.
28. Blackwood, B.P.; Yuan, C.Y.; Wood, D.R.; Nicolas, J.D.; Grothaus, J.S.; Hunter, C.J. Probiotic Lactobacillus Species Strengthen Intestinal Barrier Function and Tight Junction Integrity in Experimental Necrotizing Enterocolitis. J Probiotics Health 2017, 5, doi:10.4172/2329-8901.1000159.
29. Samak, G.; Rao, R.; Rao, R. Lactobacillus Casei and Epidermal Growth Factor Prevent Osmotic Stress-Induced Tight Junction Disruption in Caco-2 Cell Monolayers. Cells 2021, Vol. 10, Page 3578 2021, 10, 3578, doi:10.3390/CELLS10123578.
30. Abuja, P.M.; Vinelli, V.; Biscotti, P.; Martini, D.; del Bo', C.; Marino, M.; Meroño, T.; Nikoloudaki, O.; Calabrese, F.M.; Turroni, S.; et al. Effects of Dietary

Fibers on Short-Chain Fatty Acids and Gut Microbiota Composition in Healthy Adults: A Systematic Review. Nutrients 2022, Vol. 14, Page 2559 2022, 14, 2559, doi:10.3390/NU14132559.
31. Xu, T.; Wu, X.; Liu, J.; Sun, J.; Wang, X.; Fan, G.; Meng, X.; Zhang, J.; Zhang, Y. The Regulatory Roles of Dietary Fibers on Host Health via Gut Microbiota-Derived Short Chain Fatty Acids. Curr Opin Pharmacol 2022, 62, 36–42, doi:10.1016/J.COPH.2021.11.001.
32. Ortiz-Alvarez, L.; Xu, H.; Martinez-Tellez, B. Influence of Exercise on the Human Gut Microbiota of Healthy Adults: A Systematic Review. Clin Transl Gastroenterol 2020, 11, e00126, doi:10.14309/CTG.0000000000000126.
33. Ghosh, S.; Whitley, C.S.; Haribabu, B.; Jala, V.R. Regulation of Intestinal Barrier Function by Microbial Metabolites. Cell Mol Gastroenterol Hepatol 2021, 11, 1463, doi:10.1016/J.JCMGH.2021.02.007.
34. Hawley, J.A. Microbiota and Muscle Highway — Two Way Traffic. Nature Reviews Endocrinology 2019 16:2 2019, 16, 71–72, doi:10.1038/s41574-019-0291-6.
35. Bongiovanni, T.; Yin, M.O.L.; Heaney, L.M. The Athlete and Gut Microbiome: Short-Chain Fatty Acids as Potential Ergogenic Aids for Exercise and Training. Int J Sports Med 2021, 42, 1143–1158, doi:10.1055/A-1524-2095.
36. Antonini, M.; Conte, M. lo; Sorini, C.; Falcone, M. How the Interplay between the Commensal Microbiota, Gut Barrier Integrity, and Mucosal Immunity Regulates Brain Autoimmunity. Front Immunol 2019, 10, 1937, doi:10.3389/FIMMU.2019.01937/BIBTEX.
37. Cai, Y.; Folkerts, J.; Folkerts, G.; Maurer, M.; Braber, S. Microbiota-dependent and -independent Effects of Dietary Fiber on Human Health. Br J Pharmacol 2019, bph.14871, doi:10.1111/bph.14871.
38. Xu, Y.; Zhu, Y.; Li, X.; Sun, B. Dynamic Balancing of Intestinal Short-Chain Fatty Acids: The Crucial Role of Bacterial Metabolism. Trends Food Sci Technol 2020, 100, 118–130, doi:10.1016/J.TIFS.2020.02.026.
39. Brownlie, E.J.E.; Chaharlangi, D.; Wong, E.O.Y.; Kim, D.; Navarre, W.W. Acids Produced by Lactobacilli Inhibit the Growth of Commensal Lachnospiraceae and S24-7 Bacteria. Gut Microbes 2022, 14, doi:10.1080/19490976.2022.2046452/SUPPL_FILE/KGMI_A_2046452_SM4942.ZIP.
40. Hamer, H.M.; Jonkers, D.M.A.E.; Bast, A.; Vanhoutvin, S.A.L.W.; Fischer, M.A.J.G.; Kodde, A.; Troost, F.J.; Venema, K.; Brummer, R.J.M. Butyrate Modulates

Oxidative Stress in the Colonic Mucosa of Healthy Humans. Clinical Nutrition 2009, 28, 88–93, doi:10.1016/j.clnu.2008.11.002.
41. Nielsen, D.S.G.; Jensen, B.B.; Theil, P.K.; Nielsen, T.S.; Knudsen, K.E.B.; Purup, S. Effect of Butyrate and Fermentation Products on Epithelial Integrity in a Mucus-Secreting Human Colon Cell Line. J Funct Foods 2018, 40, 9–17, doi:10.1016/J.JFF.2017.10.023.
42. Gizard, F.; Fernandez, A.; de Vadder, F. Interactions between Gut Microbiota and Skeletal Muscle. Nutr Metab Insights 2020, 13, doi:10.1177/1178638820980490/ASSET/IMAGES/LARGE/10.1177_1178638820980490-FIG1.JPEG.
43. Maruta, H.; Yamashita, H. Acetic Acid Stimulates G-Protein-Coupled Receptor GPR43 and Induces Intracellular Calcium Influx in L6 Myotube Cells. PLoS One 2020, 15, e0239428, doi:10.1371/JOURNAL.PONE.0239428.
44. Zhang, B.; Liu, H.; Liu, M.; Yue, Z.; Liu, L.; Fuchang, L. Exogenous Butyrate Regulates Lipid Metabolism through GPR41-ERK-AMPK Pathway in Rabbits. https://doi-org.proxy.library.uu.nl/10.1080/1828051X.2022.2049985 2022, 21, 473–487, doi:10.1080/1828051X.2022.2049985.
45. Christiansen, C.B.; Gabe, M.B.N.; Svendsen, B.; Dragsted, L.O.; Rosenkilde, M.M.; Holst, J.J. The Impact of Short-Chain Fatty Acids on Glp-1 and Pyy Secretion from the Isolated Perfused Rat Colon. Am J Physiol Gastrointest Liver Physiol 2018, 315, G53–G65, doi:10.1152/AJPGI.00346.2017/ASSET/IMAGES/LARGE/ZH30041874330006.JPEG.
46. Grasset, E.; Puel, A.; Charpentier, J.; Collet, X.; Christensen, J.E.; Tercé, F.; Burcelin, R. A Specific Gut Microbiota Dysbiosis of Type 2 Diabetic Mice Induces GLP-1 Resistance through an Enteric NO-Dependent and Gut-Brain Axis Mechanism. Cell Metab 2017, 25, 1075-1090.e5, doi:10.1016/J.CMET.2017.04.013.
47. Kim, M.H.; Kang, S.G.; Park, J.H.; Yanagisawa, M.; Kim, C.H. Short-Chain Fatty Acids Activate GPR41 and GPR43 on Intestinal Epithelial Cells to Promote Inflammatory Responses in Mice. Gastroenterology 2013, 145, 396-406.e10, doi:10.1053/J.GASTRO.2013.04.056.
48. Lin, R.; Liu, W.; Piao, M.; Zhu, H. A Review of the Relationship between the Gut Microbiota and Amino Acid Metabolism. Amino Acids 2017, 49, 2083–2090, doi:10.1007/S00726-017-2493-3/FIGURES/1.
49. Scheiman, J.; Luber, J.M.; Chavkin, T.A.; MacDonald, T.; Tung, A.; Pham, L.D.; Wibowo, M.C.; Wurth, R.C.; Punthambaker, S.; Tierney, B.T.; et al. Meta-Omics Analysis of Elite Athletes Identifies a Performance-Enhancing Microbe That

Functions via Lactate Metabolism. Nature Medicine 2019 25:7 2019, 25, 1104–1109, doi:10.1038/s41591-019-0485-4.
50. Odriozola, C.P.; Cordero, J.Á.G.; Daura, J.; Sanz, M.; Martínez-Blanes, J.M.; Avilés, M.Á. Reliability of Blood Lactate as a Measure of Exercise Intensity in Different Strains of Mice during Forced Treadmill Running. PLoS One 2019, 14, e0215584, doi: 10.1371/JOURNAL.PONE.0215584.

Supplementary Information

Supplementary methods

Animals and experimental design

Male C57BL/6J mice at 9 weeks of age were ordered from Charles River (Sulzfeld, Germany). The mice were randomly divided into the following groups: control (CON, n = 60), moderate treadmill exercise training (MOD-EX, n = 60), and vigorous treadmill exercise training (VIG-EX, n = 60). In each group, the mice were randomly divided into 3 subgroups by their euthanasia time points: 2, 4 and 6 weeks of intervention (n = 20, respectively). Per subgroup, the mice were housed in 5 standard cages with 4 mice each and maintained at 21°C with 55% humidity on a 12 h light/dark cycle in a specific pathogen-free barrier facility and had ad libitum access to a standard chow diet [RM3 (P), Special Diet Services, UK], along with pathogen-free water. The ingredients of the diet are listed in Supplementary Table S1. Food intake per cage and body weight were assessed once a week.

Rectal temperature

Rectal temperature was measured weekly using a digital thermometer (BAT-12, Physitemp Instruments, USA). The probe was gently inserted to a depth of 1 cm into the mouse rectum 15 min after the treadmill running session. Before each insertion, the probe was sterilized with 75% ethanol.

Treadmill running exercise protocol

A 3-day progressive exercise training regime was adapted to familiarize the MOD-EX and VIG-EX mice to the 5-lane rodent treadmill (Maze Engineers, USA) where the speed and incline of the track were incrementally increased. 4 mice per group were allowed to run together on one treadmill lane. No electric shocks were used throughout the running sessions, instead the mice were gently nudged back on the belt with a brush when they dropped off the track. Starting from day 4, the mice followed a fixed training regime, adapted from previous studies [1,2]. The MOD-EX group was trained 5 times per week for 60 min including a 15 min warm-up at 6-16 m/min and 45 min at 16 m/min with a 5° incline of the track. The VIG-EX group was trained 3 times per week for 30 min including a 5 min warm-up at 6-23 m/min and 25 min at 23 m/min with a 5° incline of the track. To ensure that the exercise straining remained strenuous, starting from day 15, the running speed of

the MOD-EX group and the VIG-EX group was increased by 1 m/min (up to 17 m/min and 24 m/min, respectively). Starting from day 29, the speed of the VIG-EX group was increased further to 25 m/min. The detailed treadmill program is listed as Supplementary Table S2 and S3. In total, the mice were trained for 2, 4 or 6 weeks. The outline of the time points for exercise training, rest and sacrifice are depicted in Supplementary Fig. S1. Each time the mice in the MOD-EX and VIG-EX groups were trained, the mice in the CON group were also handled and stroked as a control for the stress that the exercising mice experienced.

Euthanasia and intestinal fluorescein permeability

Referring to Nascimento et al. [3] and Woting et al. [4], immediately after the last treadmill training session, FITC-dextran (FD; 4 kDa, 46944, Sigma-Aldrich, USA) was administered to each mouse by oral gavage (500 mg/kg BW). Since the mice had to perform the last training session 1 h before sacrifice, the animals were not fasted prior to euthanasia. Blood was collected by retro-orbital bleeding immediately before euthanasia under isoflurane anaesthesia 1 h after the gavage. Serum separator clot activator tubes (Greiner Bio-One, Italy) were used for blood collection and serum was isolated after centrifugation (1500 × g) and diluted 1:5 (v/v, FD) in sterile phosphate-buffered saline (PBS). Fluorescence intensity was measured spectrophotometrically (λex 485 nm, λem 535 nm for FD) with a fluorescent microplate reader (GloMax Discover, Promega, USA) in black-wall 96-well plates. The fluorescent emission intensity was converted into fluorescein flux per hour with the help of FD standard curves.

Tissue collection and treatment

Two cm of the segments from the proximal, middle and distal parts of the small intestine, and from the colon were isolated and cleaned with ice cold sterile PBS. The spleen was harvested and weighed. Tissue samples were snap-frozen on dry ice and stored at −80°C until future use.

According to Carol et al. [5], Swiss rolls were made from around 5 cm proximal small intestine (starting from ca. 4 cm to the pylorus), distal small intestine (till ca. 2 cm to the cecum) and colon (starting from ca. 2 cm to the cecum). The Swiss rolls were fixed in cold 3.7% formaldehyde solution (104003, Sigma-Aldrich, USA) for 48 h, transferred to 70% ethanol, dehydrated using a series of increasing

ethanol concentrations, cleared with xylene, and then embedded in paraffin blocks for histomorphological evaluation.

Western blotting

The colonic segments were lysed and homogenized by Precellys 24 homogenizer (Bertin Instruments, France) using Precellys lysing beads at 6000 rpm (10 s × 3 cycles) with cold Pierce RIPA buffer (Thermo Fisher Scientific, USA) containing a protease inhibitor cocktail (#11836170001, Roche, Switzerland). Total protein concentration was assessed and standardized with Pierce BCA Protein Assay Kit (Thermo Fisher Scientific, USA).

Equal amounts (50 µg) of boiled protein samples were separated by electrophoresis (Criterion Gel, 4-20% Tris-HCL, Bio-Rad, USA) and transferred onto Trans-Blot Turbo polyvinylidene difluoride (PVDF) membranes (midi format 0.2 µm, Bio-Rad, USA). After being blocked with 5% skimmed milk in PBS containing 0.05% Tween-20 (PBST), the membranes were incubated overnight at 4℃ with the primary antibodies of HSP-70 (1:1000, #C92F3A-5, Enzo life science, Belgium), HSF-1 (1:1000, #D3L8I, Cell Signaling, USA), occludin (1:500, #404700, Invitrogen, USA), claudin-3 (1:1000, #341700, Invitrogen, USA), ZO-1 (1:500, #339100, Invitrogen, USA), GPR41 (1:2000, #ab238854, Abcam, UK) and GPR43 (1:400, #PA5-111780, Invitrogen, USA), then incubated with correspondent horseradish peroxidase (HRP)-conjugated secondary antibodies (1:10,000, Dako, Denmark) for 2 h at room temperature. After being rinsed with PBST and incubated with ECL detection reagent (#RPN2235, GE Healthcare, USA), the membranes were exposed to the ECL imaging system (ChemiDoc MP, Bio-Rad, USA). The optical intensity of the blots was recorded and analysed by using Image Lab (version 6.01, Bio-Rad, USA) and ImageJ (version 1.80, NIH, USA) software. Housekeeping protein β-actin (1:2000, #13E5, Cell Signaling, USA) was assessed in parallel with each target protein and used for normalization. The blots on the same membrane were stripped by Restore PLUS Western Blot Stripping Buffer (Thermo Fisher Scientific, USA) and re-blotted.

Histomorphological evaluation

The Swiss rolls of proximal and distal parts of the small intestine and colonic parts were cut into 5 µm sections and stained with hematoxylin and eosin (H&E). The epithelial morphology, mucosal architecture and inflammation of the intestinal

samples were evaluated and scored by double-blinded technicians, according to the modification of Erben et al. [6]. One random field per section (3 sections per animal) of the same animal were scored. The scoring scheme is listed in Supplementary Table S4 and S5. Three main categories were evaluated: inflammatory cell infiltrates, epithelial changes, and mucosal architecture status, with specified criteria for each category. The villus length was measured using Fiji of ImageJ software (NIH, USA). From the three fields per animal, three random villi per field were measured and average villus length is shown. After being stained with Alcian Blue and Nuclear Fast Red, the goblet cells in each villus were located and counted. The ratio of goblet cells to all enterocytes on the same villus represented the percentage of villous goblet cells.

Immunofluorescence staining

Localization of TJ/AJ proteins was determined by immunofluorescence staining. The sections were incubated for 30 min with 0.3% H2O2 solution in methanol to block endogenous peroxidase activity. After gradient rehydration, the slides were rinsed by PBS and incubated in boiling sodium citrate buffer (pH 6.0) for 10 min, then cooled down for 1 h in the buffer. The slides were rinsed, blocked with 5% goat serum in PBS containing 1% bovine serum albumin (BSA) for 30 min at room temperature, and incubated overnight with primary antibody against occludin (1:100, #404700, Invitrogen, USA) at 4 °C. After incubation with the primary antibodies, the slides were rinsed and incubated with Alexa-Fluor fluorescently conjugated secondary antibody (goat anti-rabbit IgG, 1:1000, Invitrogen, USA) for 1 h at room temperature. The slides were mounted, and the nuclei were counterstained with ProLong Gold Antifade Mountant with DAPI (#P36935, Invitrogen, USA) and cells were visualized by a confocal microscopy system (TCS SP8, Leica, Germany). Rabbit IgG polyclonal isotype control (#ab176094, Abcam, UK) was used for the occludin antibody listed above. Isotype control and secondary antibody control of the immunofluorescence staining are depicted in Supplementary Fig. S2.

Caecal metabolomics measurement

The concentrations of SCFAs and amino acids (AAs) in the caecal contents were quantified by nuclear magnetic resonance (NMR) spectroscopy, adapted from the protocol developed by Kim et al. [7] for faecal samples.

Each sample tube was weighed before sample preparation. To each sample 50 µl of 0.5 mm zirconium oxide beads (Next Advance, USA) ceramic beads and 500 µl of pH 7.4 potassium phosphate buffer (0.15 M) containing 0.2 mM NaN3 were added. Then, the tubes were subjected to bead beating for 30 seconds. The tubes were subsequently centrifuged at 18,000 × g at 4 °C for 15 minutes. 300 µl of supernatant was transferred to new 1.5 ml Eppendorf tubes and centrifuged at 18,000 × g at 4°C for 1 h. 225 µl of supernatant was added to 25 µl of 100% D2O containing 4 mM TSP-d4, and 6 mM dimethylsulfone (DMSO). A customized Gilson 215 liquid handler was used to transfer the samples to a 3.0 mm Bruker NMR tube rack. The original sample tubes were cleaned, dried and weighed again. 1H NMR data were collected using a Bruker 600 MHz Avance Neo/IVDr spectrometer (Bruker Scientific Instruments, USA) equipped with a 5 mm TCI cryogenic probe head and a z-gradient system. A Bruker SampleJet sample changer was used for sample insertion and removal. All experiments were recorded at 300 K. A standard sample of 99.8% methanol-d4 was used for temperature calibration before each batch of measurements [8]. One-dimensional (1D) 1H NMR spectra were recorded using the first increment of a NOESY pulse with presaturation (γB1 = 50 Hz) during a relaxation delay of 4 s and a mixing time of 10 ms for efficient water suppression [9,10]. Initial shimming was performed using the TopShim tool on a random mix of urine samples from the study, and subsequently the axial shims were optimized automatically before every measurement. Duration of 90° pulses were automatically calibrated for each individual sample using a homonuclear-gated mutation experiment on the locked and shimmed samples after automatic tuning and matching of the probe head [11]. 16 scans of 65,536 points covering 12,335 Hz were recorded. The Free Induction Decay of the 1D experiment was zero-filled to 65,536 complex points prior to Fourier transformation. An exponential window function was applied with a line-broadening factor of 0.3 Hz. The spectra were automatically phase and baseline corrected and automatically referenced to an internal standard (TSP = 0.0 ppm).

Metabolites were quantified in a select number of spectra using the Chenomx NMR Suite (version 8.6, Chenomx, Canada) and by fitting the remaining spectra automatically in the KIMBLE environment [12]. The areas were converted concentrations using the DMSO internal standard.

DNA extraction of caecal contents and library construction

Caecal contents were collected from individual mice and stored at −80°C until future use. Total DNA extraction and library construction were performed by BGI Genomics (Shenzhen, China). Total bacterial DNA was extracted using the MagPure Stool DNA KF Kit B (MD5115, Magen, China) following the manufacturer's instructions. DNA was quantified with the Qubit Fluorometer (Invitrogen, USA) by using Qubit dsDNA BR Assay Kit (Q32850, Invitrogen, USA) and the quality was checked by running an aliquot on 1% agarose gel electrophoresis.

The variable regions V3-V4 of the bacterial 16S rRNA gene were amplified with degenerate PCR primers 341F (5'-ACTCCTACGGGAGGCAGCAG-3') and 806R (5'-GGACTACHVGGGTWTCTAAT-3'). Both forward and reverse primers were tagged with Illumina adapter, pad and linker sequences. PCR enrichment was performed in a 50 µl reaction containing 30 ng template, fusion PCR primers and PCR master mix. PCR cycling conditions were as follows: 94 ℃ for 3 minutes, 30 cycles of 94 ℃ for 30 seconds, 56℃ for 45 seconds, 72℃ for 45 seconds and final extension for 10 minutes at 72℃ for 10 minutes. The PCR products were purified with AMPure XP beads (A63882, Beckman Coulter, USA) and eluted in elution buffer. Libraries were qualified by Agilent 2100 Bioanalyzer (Agilent, USA).

Gut microbiota sequencing and bioinformatics analysis

The validated libraries were used for sequencing by BGI Genomics (Shenzhen, China) on the Illumina HiSeq 2500 platform (Illumina, San Diego, California) following the standard pipelines of Illumina, and generating 2 × 300 bp paired end reads with a coverage of 50k reads. Raw reads were filtered to remove adaptors and low-quality and ambiguous bases, and then paired-end reads were added to tags by the Fast Length Adjustment of Short reads program (FLASH, version 1.2.11) to get the tags. The tags were trimmed to 400 bp and denoised into amplicon sequence variants (ASVs) using the Deblur plugin [13] of QIIME 2 (2022.2.0) and chimera sequences were compared and removed. Then, ASV representative sequences were taxonomically classified using QIIME 2 with a weighted (on distal animal gut) naive Bayes classifier trained on Silva 138.1 database [14–17]. ASV representative sequences were also aligned to infer phylogenies using the Multiple Alignment using Fast Fourier Transform (MAFFT) algorithm via the phylogeny plugin [18] of QIIME 2. The feature table, taxonomy mapping and phylogenetic trees were analysed using qiime2R (0.99.6), phyloseq (1.40.0) and

microbiome (1.18.0) packages based on R 4.2.0, for relative abundance, alpha diversity, and beta diversity results. The data were visualized using ggplot2 (3.3.6) R package. LEfSe analyses was performed using the Galaxy computational tool (https://huttenhower.sph.harvard.edu/galaxy/) with the help of the phyloseqCompanion (0.3.3) and microbiomeMarker (1.2.1) R packages [19].

Serum cytokines and chemokines concentrations

Serum granulocyte colony-stimulating factor (G-CSF), chemokine (C-X-C motif) ligand (CXCL) 1 [also referred to as KC or growth-regulated oncogene (GRO)-α], CXCL2, chemokine (C-C motif) ligand (CCL) 2 [also referred to as monocyte chemoattractant protein (MCP)-1], interleukin (IL)-1β, IL-4, IL-6, IL-10, IL-13 and tumour necrosis factor (TNF)-α were measured by a Luminex bead-based multiplex system (PPX-10-MX47XEM, Thermo Fisher Scientific, USA) according to the manufacturer's protocol.

Serum C-reactive protein (CRP) was measured by a Mouse C-Reactive Protein DuoSet Enzyme-linked Immunosorbent Assay (ELISA) kit (DY1829, R&D Systems, USA), following the manufacturer's protocol. Serum was diluted 1:100 (v/v) with 1% bovine serum albumin (BSA, A9647, Sigma-Aldrich, USA) in PBS. The optical density of each well was determined by a microplate reader (GloMax Discover, Promega, USA) at 450 nm/560 nm. The absorbance was converted into concentration with the help of CRP standard curves.

Statistical analysis

Statistical analyses were performed by using GraphPad Prism software (version 9.3.1, GraphPad, USA) or the functions of R packages (for Pearson's correlation coefficient calculation and microbiome analysis). Differences between groups were determined with parametric repeated measures (RM) two-way analysis of variance (ANOVA) (for body weight, food intake and rectal temperature measures), or ordinary one-way ANOVA (for non-repeated measures, such as FITC-dextran permeability, relative intensities of WB bands, morphological scores, etc.) with Bonferroni post-hoc test, or non-parametric Kruskal-Wallis rank-sum test, two-sided Welch's test or permutational multivariate analysis of variance (PERMANOVA) (for microbiome analyses). A Pearson rank correlation test was conducted to examine associations between the parameters tested, with

coefficient |R| > 0.4 being considered correlated. Results were considered statistically significant when $p < 0.05$ or corrected $q < 0.05$.

References

1. Billat, V.L.; Mouisel, E.; Roblot, N.; Melki, J. Inter- and Intrastrain Variation in Mouse Critical Running Speed. https://doi.org/10.1152/japplphysiol.00991.2004 2005, doi:10.1152/JAPPLPHYSIOL.00991.2004.
2. Sato, S.; Basse, A.L.; Schönke, M.; Chen, S.; Samad, M.; Altıntaş, A.; Laker, R.C.; Dalbram, E.; Barrès, R.; Baldi, P.; et al. Time of Exercise Specifies the Impact on Muscle Metabolic Pathways and Systemic Energy Homeostasis. Cell Metab 2019, 30, 92-110.e4, doi:10.1016/J.CMET.2019.03.013.
3. Nascimento, J.C.; Matheus, V.A.; Oliveira, R.B.; Tada, S.F.S.; Collares-Buzato, C.B. High-Fat Diet Induces Disruption of the Tight Junction-Mediated Paracellular Barrier in the Proximal Small Intestine Before the Onset of Type 2 Diabetes and Endotoxemia. Dig Dis Sci 2021, 66, 3359–3374, doi:10.1007/S10620-020-06664-X/FIGURES/9.
4. Woting, A.; Blaut, M. Small Intestinal Permeability and Gut-Transit Time Determined with Low and High Molecular Weight Fluorescein Isothiocyanate-Dextrans in C3H Mice. Nutrients 2018, 10, doi:10.3390/NU10060685.
5. Park, C.M.; Reid, P.E.; Walker, D.C.; MacPherson, B.R. A Simple, Practical 'Swiss Roll' Method of Preparing Tissues for Paraffin or Methacrylate Embedding. J Microsc 1987, 145, 115–120, doi:10.1111/J.1365-2818.1987.TB01321.X.
6. Erben, U.; Loddenkemper, C.; Doerfel, K.; Spieckermann, S.; Haller, D.; Heimesaat, M.M.; Zeitz, M.; Siegmund, B.; Ku¨hl, A.A. A Guide to Histomorphological Evaluation of Intestinal Inflammation in Mouse Models. Int J Clin Exp Pathol 2014, 7, 4557.
7. Kim, H.K.; Kostidis, S.; Choi, Y.H. NMR Analysis of Fecal Samples. Methods in Molecular Biology 2018, 1730, 317–328, doi:10.1007/978-1-4939-7592-1_24.
8. Findeisen, M.; Brand, T.; Berger, S. A 1H-NMR Thermometer Suitable for Cryoprobes. Magn Reson Chem 2007, 45, 175–178, doi:10.1002/MRC.1941.
9. Kumar, A.; Ernst, R.R.; Wüthrich, K. A Two-Dimensional Nuclear Overhauser Enhancement (2D NOE) Experiment for the Elucidation of Complete Proton-Proton Cross-Relaxation Networks in Biological Macromolecules. Biochem Biophys Res Commun 1980, 95, 1–6, doi:10.1016/0006-291X(80)90695-6.

10. Price, W.S. Water Signal Suppression in NMR Spectroscopy. Annu Rep NMR Spectrosc 1999, 38, 289–354, doi:10.1016/S0066-4103(08)60040-X.
11. Wu, P.S.C.; Otting, G. Rapid Pulse Length Determination in High-Resolution NMR. Journal of Magnetic Resonance 2005, 176, 115–119, doi:10.1016/J.JMR.2005.05.018.
12. Verhoeven, A.; Giera, M.; Mayboroda, O.A. KIMBLE: A Versatile Visual NMR Metabolomics Workbench in KNIME. Anal Chim Acta 2018, 1044, 66–76, doi:10.1016/J.ACA.2018.07.070.
13. Amir, A.; McDonald, D.; Navas-Molina, J.A.; Kopylova, E.; Morton, J.T.; Zech Xu, Z.; Kightley, E.P.; Thompson, L.R.; Hyde, E.R.; Gonzalez, A.; et al. Deblur Rapidly Resolves Single-Nucleotide Community Sequence Patterns. mSystems 2017, 2, doi:10.1128/MSYSTEMS.00191-16/SUPPL_FILE/SYS002172091SF3.PDF.
14. Quast, C.; Pruesse, E.; Yilmaz, P.; Gerken, J.; Schweer, T.; Yarza, P.; Peplies, J.; Glöckner, F.O. The SILVA Ribosomal RNA Gene Database Project: Improved Data Processing and Web-Based Tools. Nucleic Acids Res 2013, 41, doi:10.1093/NAR/GKS1219.
15. Robeson, M.S.; O'Rourke, D.R.; Kaehler, B.D.; Ziemski, M.; Dillon, M.R.; Foster, J.T.; Bokulich, N.A. RESCRIPt: Reproducible Sequence Taxonomy Reference Database Management. PLoS Comput Biol 2021, 17, e1009581, doi:10.1371/JOURNAL.PCBI.1009581.
16. Kaehler, B.D.; Bokulich, N.A.; McDonald, D.; Knight, R.; Caporaso, J.G.; Huttley, G.A. Species Abundance Information Improves Sequence Taxonomy Classification Accuracy. Nature Communications 2019 10:1 2019, 10, 1–10, doi:10.1038/s41467-019-12669-6.
17. Bokulich, N.A.; Kaehler, B.D.; Rideout, J.R.; Dillon, M.; Bolyen, E.; Knight, R.; Huttley, G.A.; Gregory Caporaso, J. Optimizing Taxonomic Classification of Marker-Gene Amplicon Sequences with QIIME 2's Q2-Feature-Classifier Plugin. Microbiome 2018, 6, 1–17, doi:10.1186/S40168-018-0470-Z/TABLES/3.
18. Katoh, K.; Standley, D.M. MAFFT Multiple Sequence Alignment Software Version 7: Improvements in Performance and Usability. Mol Biol Evol 2013, 30, 772–780, doi:10.1093/MOLBEV/MST010.
19. Segata, N.; Izard, J.; Waldron, L.; Gevers, D.; Miropolsky, L.; Garrett, W.S.; Huttenhower, C. Metagenomic Biomarker Discovery and Explanation. Genome Biol 2011, 12, doi:10.1186/GB-2011-12-6-R60.

Supplementary figures:

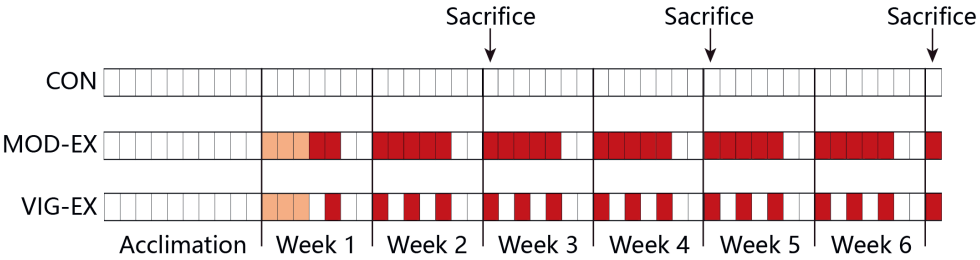

Figure S1. Schematic diagram of the treadmill training protocol. Each box of the grid represents one day, white boxes stand for rest days, light red boxes for the 3-day progressive adaptation period, and dark red boxes for training days. The mice were sacrificed at different timepoint after the training (arrows). CON, Control; MOD-EX: moderate exercise; VIG-EX: vigorous exercise.

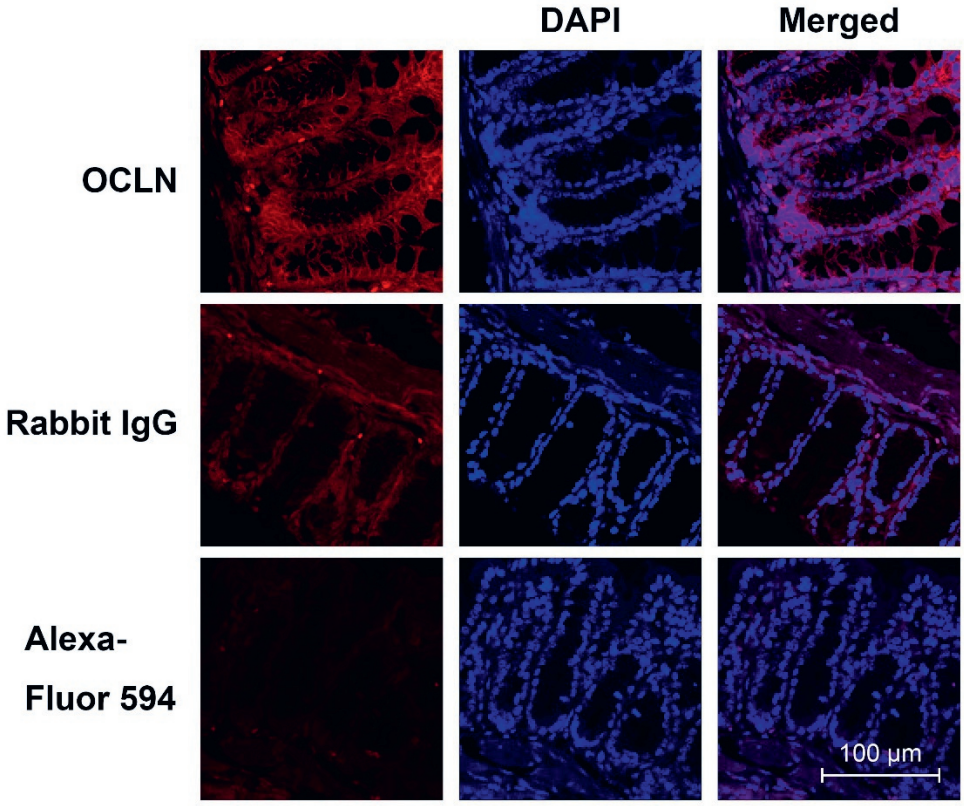

Figure S2. Isotype control and secondary antibody control of the immunofluorescence staining. The results were acquired by Leica TCS SP8 confocal microscope with HCX IRAPO L 25×/0.95 objective lens at 2.25× digital magnification; pinhole: 1.50 AU. Red colour: fluorescent signals from Alexa-Fluor® 594 secondary antibodies; blue colour: DAPI located nuclei. OCLN: occludin.

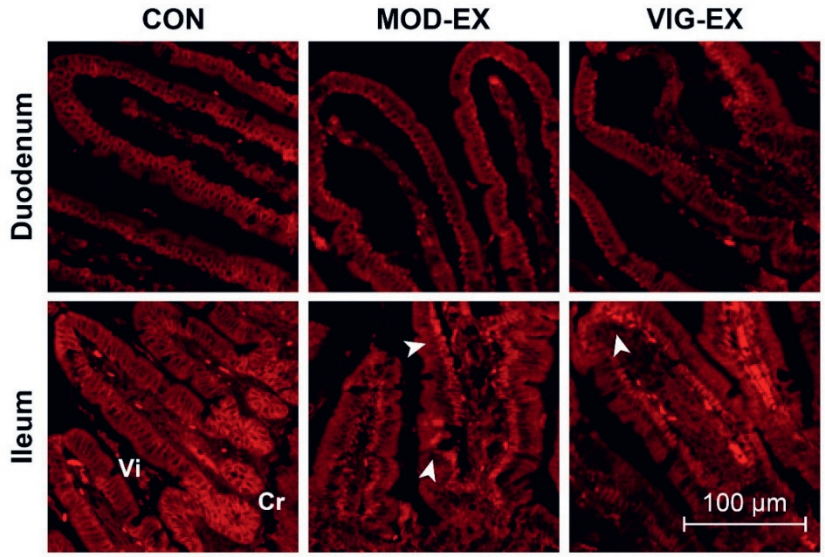

Figure S3. Immunofluorescence staining of duodenal (proximal small intestine) and ileal (distal small intestine) occludin protein. OCLN localized at the cell membrane showed continuous chain-like structures forming the rim of normal duodenal and ileal villi. These chain-like structures in duodenal and ileal tissue were less clear in both exercise groups. Stronger OCLD expression was observed in the control ileal crypts (Cr) than in villi (Vi), which is less clear after exercise. In addition, OCLN tended to aggregate on the lamina propria side of the duodenum and ileum of strenuous exercise-trained mice (arrow heads). The results were acquired by Leica TCS SP8 confocal microscope with HCX IRAPO L 25×/0.95 objective lens at 2.25× digital magnification; pinhole: 1.50 AU. Red colour: fluorescent signals from Alexa-Fluor® 594 secondary antibodies; arrow head: aggregative dislocation of occludin. CON: Control; MOD-EX: moderate exercise; VIG-EX: vigorous exercise.

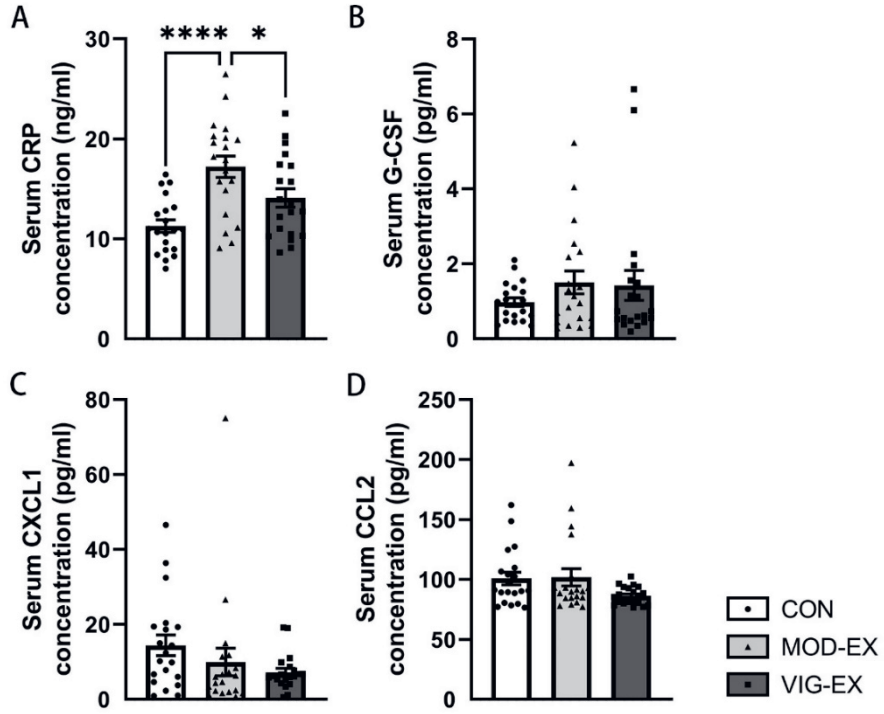

Figure S4. The effect of strenuous exercise training on serum CRP, cytokine, and chemokine levels. Concentrations of serum CRP (**A**), G-CSF (**B**), CXCL1 (**C**) and CCL2 (**D**) after 6 weeks of moderate or vigorous exercise were assessed by Luminex assay. Data are presented as mean ± SEM; n = 20 per group. Statistical differences were analysed by one-way ANOVA followed by the Bonferroni's multiple comparison test. * $p < 0.05$, **** $p < 0.0001$. CON: Control; MOD-EX: moderate exercise; VIG-EX: vigorous exercise; CRP: C-reactive protein; G-CSF: granulocyte colony-stimulating factor; CXCL1: chemokine (C-X-C motif) ligand 1; CCL2: chemokine (C-C motif) ligand 2.

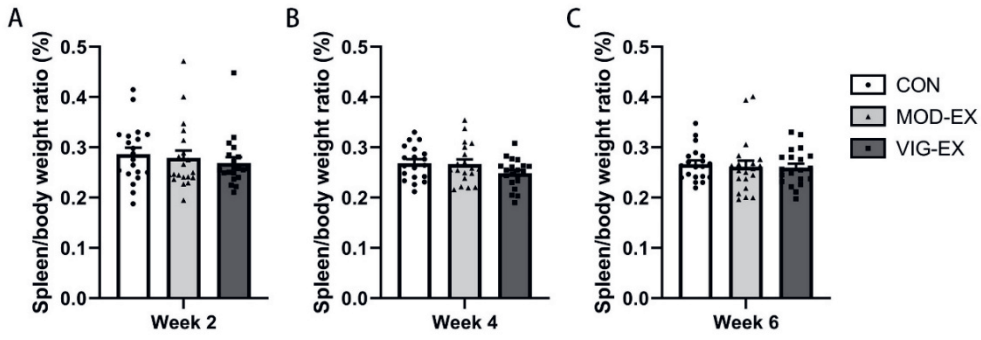

Figure S5. Spleen/body weight ratio of the mice after 2 (**A**), 4 (**B**) and 6 weeks (**C**) of moderate or vigorous exercise. Data are presented as mean ± SEM; n = 20 per group. No significant difference was observed between the groups ($p > 0.05$). CON: Control; MOD-EX: moderate exercise; VIG-EX: vigorous exercise.

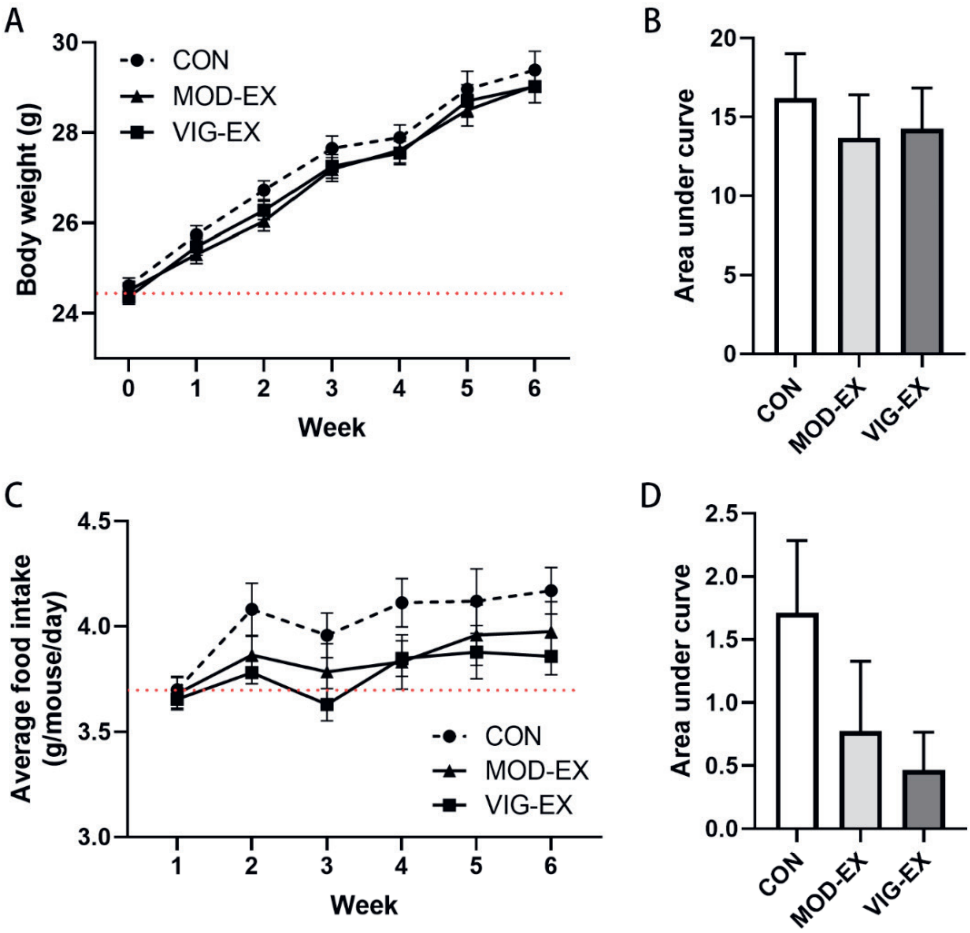

Figure S6. Effect of strenuous exercise on body weight and food intake. (**A** and **B**) Body weight gain and integral area under the curves of body weight calculated for statistical analysis. The red dotted-line represents the baseline: the average body weight of all mice at week 0 (24.63 g). Data are presented as mean ± SEM; n = 20 (individuals) per group. (**C** and **D**) Average food intake per day and integral area under the curves of food intake calculated for statistical analysis. The red dotted-line represents the baseline: the average daily food intake per mouse at week 1 of the control group (3.70 g). Data are presented as

mean ± SEM; n = 5 (cages) per group. Statistical differences were analysed by two-way repeated measures ANOVA. No significant differences of means were observed between the groups of interest ($p > 0.05$). CON: Control; MOD-EX: moderate exercise; VIG-EX: vigorous exercise.

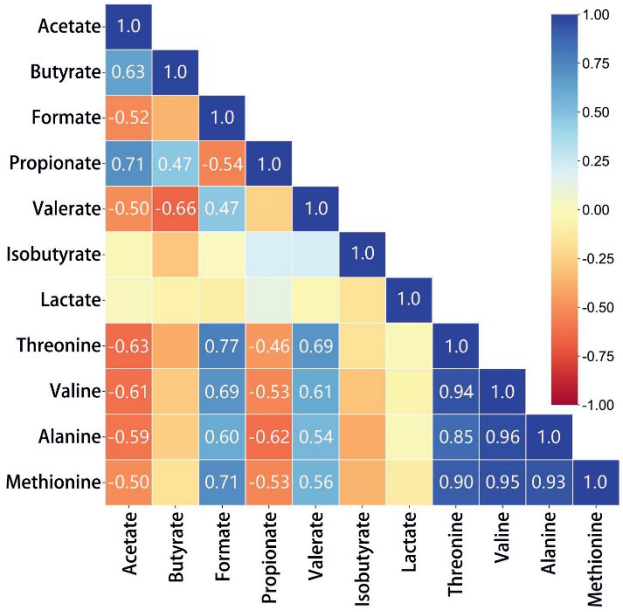

Figure S7. Pearson's correlations between caecal metabolite concentrations. Matrix heatmap indicating the Pearson's correlation coefficients between the concentrations of different caecal metabolites in all groups. Values of significant correlations are annotated in the correspondent intersections that satisfy $|R| > 0.4$ while $p < 0.05$. SCFAs: short-chain fatty acids; AAs: amino acids.

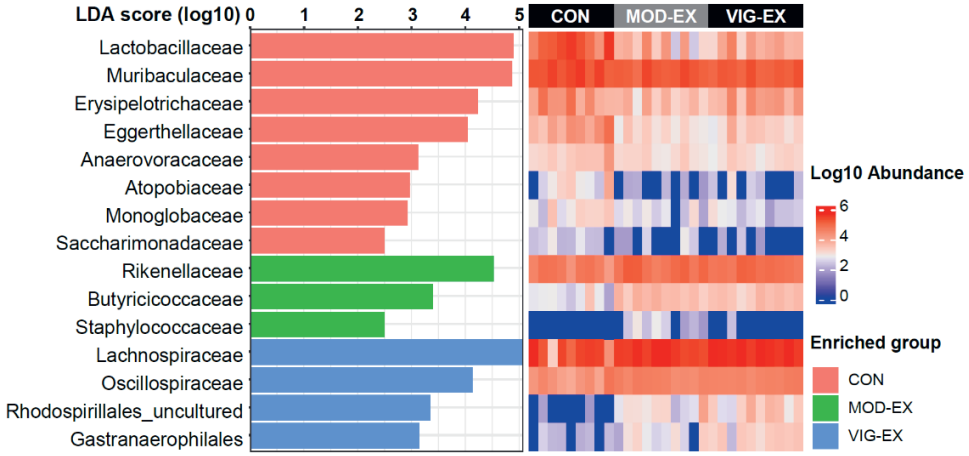

Figure S8. Bacterial families that discriminated among CON, MOD-EX and VIG-EX. LEfSe plots of taxonomic biomarkers at family level, with a heat map indicating logarithmic abundance of discriminating taxa. LEfSe algorithm was performed using relative abundance data with Kruskal-Wallis rank-sum test (α = 0.05). Features were considered discriminative at an LDA score > 2.0. LEfSe: Linear discriminant analysis with effect size; LDA: linear discriminant analysis; CON: Control; MOD-EX: moderate exercise; VIG-EX: vigorous exercise.

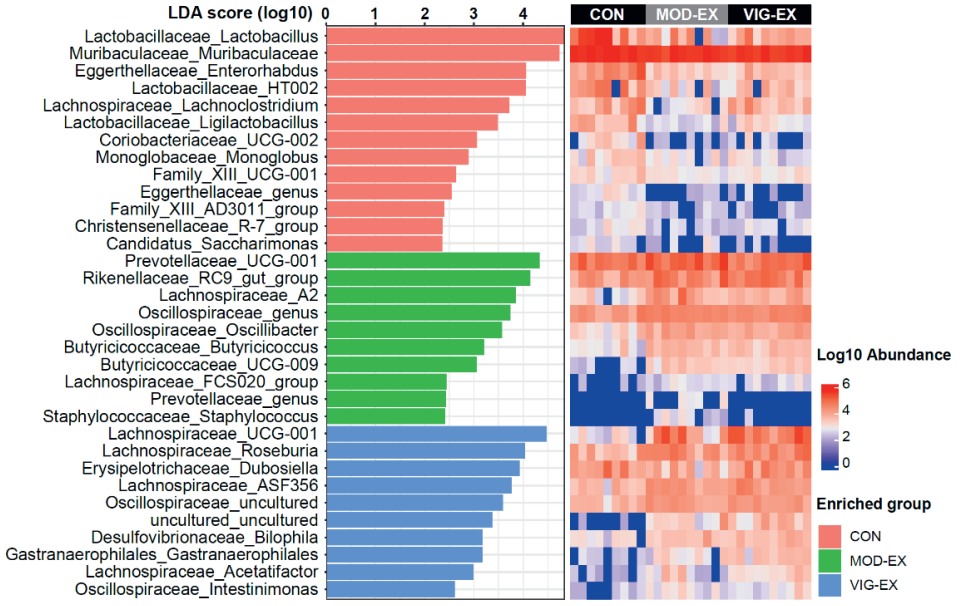

Figure S9. Bacterial geni that discriminated among CON, MOD-EX and VIG-EX. LEfSe plots of taxonomic biomarkers at genus level, with a heat map indicating logarithmic abundance of discriminating taxa. LEfSe algorithm was performed using relative abundance data with Kruskal-Wallis rank-sum test ($\alpha = 0.05$). Features were considered discriminative at an LDA score > 2.0. LEfSe: Linear discriminant analysis with effect size; LDA: linear discriminant analysis; CON: Control; MOD-EX: moderate exercise; VIG-EX: vigorous exercise.

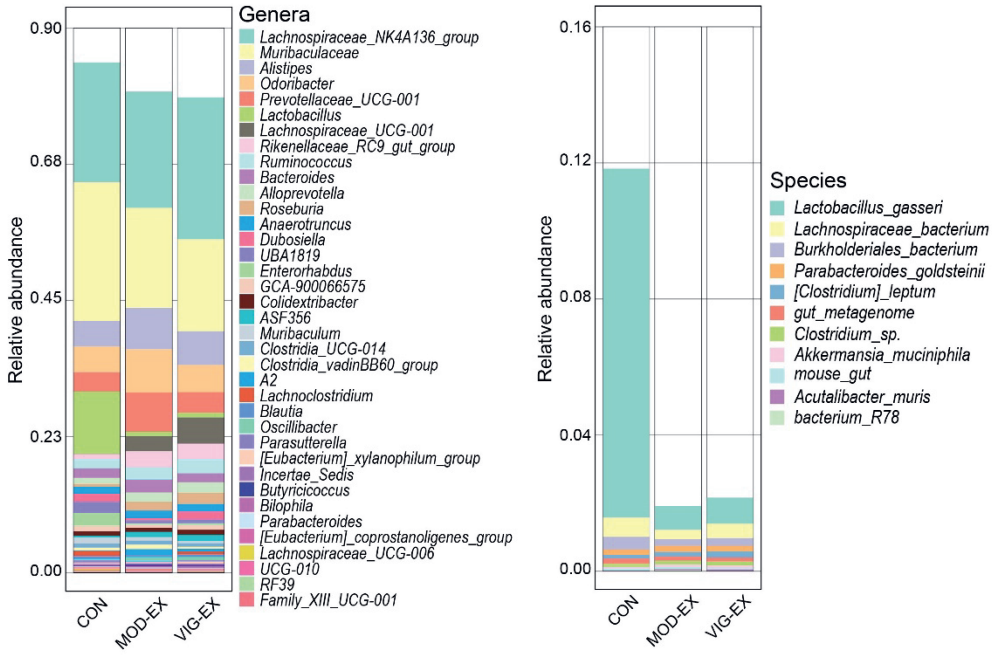

Figure S10. The effect of strenuous exercise on caecal microbiota composition. Bacterial taxonomic composition in the mouse cecum following 6 weeks of strenuous exercise training at genus and species levels. The relative abundances are displayed as mean of 9 samples (CON) or 10 samples (MOD-EX or VIG-EX) per group in the histogram in the corresponding proportion and colour according to the legend. The uncoloured proportion in includes uncultured, unidentified and unknown microorganisms. CON: Control; MOD-EX: moderate exercise; VIG-EX: vigorous exercise.

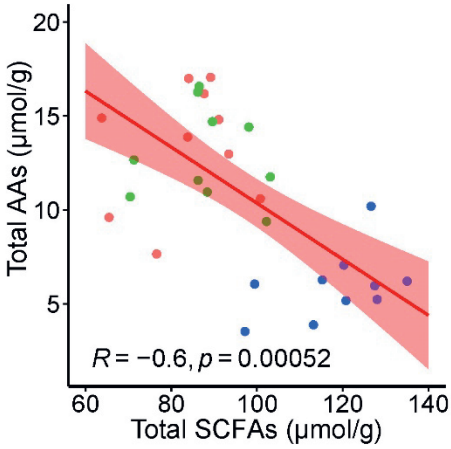

Figure S11. Pearson's correlation between the total short-chain fatty acid concentrations and total amino acid concentrations in the caecal contents of control, moderate exercise training and vigorous exercise training groups (n = 10 per group). CON: Control; MOD-EX: moderate exercise; VIG-EX: vigorous exercise; SCFAs: short-chain fatty acids; AAs: amino acids.